Multi-layer pre-vascularized magnetic cell sheets for bone regeneration

Ana S. Silva[1*], Lúcia F. Santos[1], Maria C. Mendes, João F. Mano[*]

1- Both authors had contributed equally to the preparation of the manuscript
* corresponding author: sofiamsilva@ua.pt; jmano@ua.pt

Affiliation: Department of Chemistry, CICECO–Aveiro Institute of Materials, University of Aveiro, 3810-193 Aveiro, Portugal

Abstract

The lack of effective strategies to produce vascularized 3D bone transplants *in vitro,* hampers the development of thick-constructed bone, limiting the translational of lab-based engineered system to clinical practices. Cell sheet (CS) engineering techniques provide an excellent microenvironment for vascularization since the technique can maintain the intact cell matrix, crucial for angiogenesis. In an attempt to develop hierarchical vascularized 3D cellular constructs, we herein propose the construction of stratified magnetic responsive heterotypic CS by making use of iron oxide nanoparticles previously internalized within cells. Magnetic force-based CS engineering allows for the construction of thick cellular multilayers. Results show that osteogenesis is achieved due to a synergic effect of human umbilical vein endothelial cells (HUVECs) and adipose-derived stromal cells (ASCs), even in the absence of osteogenic differentiating factors. Increased ALP activity, matrix mineralization, osteopontin and osteocalcin detection were achieved over a period of 21 days for the heterotypic CS conformation (ASCs/HUVECs/ASCs), over the homotypic one (ASCs/ASCs), corroborating our findings. Moreover, the validated crosstalk between BMP-2 and VEGF releases triggers not only the recruitment of blood vessels, as demonstrated in an *in vivo* CAM assay, as well as the osteogenesis of the 3D cell construct. The *in vivo* angiogenic profile also demonstrated preserved human vascular structures and human cells showed the ability to migrate and integrate within the chick vasculature.

Keywords

Magnetic cell sheet; scaffold-free tissue engineering; vascularization; osteogenic differentiation

1. Introduction

Tissue engineering (TE) aims to develop biological substitutes to replace, repair or regenerate lost tissue function or damaged tissues/organs.[1–5] Despite the notable advances in the field, the struggle in mimicking the complex environment of biological tissues, including vascularization, hampers the fabrication of complex organs limiting translational and clinical success.[2,3,6–8] In fact, traditional TE methods, which either focus on the injection of isolated cell suspensions or on the use of biodegradable scaffolds to support tissue formation, deprive cells of their endogenous extracellular matrix (ECM), which may dampen cell differentiation.[2] Cell-sheet (CS) technology, which has arisen as a reliable alternative to such conventional and limiting strategies,[2–5] allows for the creation of cell-dense tissues that can be harvested as a whole, preserving their ECM.[9] Upon *in vivo* transplantation, tissues fabricated by CS engineering are able to adhere to the surface of the host tissue without suture and form cell-like dense structure,[10] enabling the maintenance of cell-cell interactions that lead to a proper tissue regeneration.[1] CS technology has been applied to several types of tissues such as heart, liver, bladder, bone, cornea and esophagus,[9] with the two

latter having achieved successful clinical outcomes.[11] Yet, engineering CS for bone regeneration is still in its infancy. The difficulty in reproducing the high levels of hierarchical organization of bone, including vascularization, may hamper the development of totally functional tissues.[12–15] In fact, engineering thick tissue replacements to fit bone defects depends on rapid and sufficient vascularization in the tissue-engineered constructs, which is a pre-requisite for optimal cell survival and perfect tissue integration *in vivo*.[9] Apart from bone growth, vascularization is also involved in bone healing, both in natural and artificial bone implants.[16] Therefore, tissue ischemia and low mechanical strength of thin CS limits their application towards bone repair. Recent studies have focused on the pre-vascularization of CS for bone regeneration priori *in vivo* implantation in order to promote a vascular network using the thermo-responsive dishes of poly(N-isopropylacrylamide) (PIPAAm) proposed by Okano and co-workers.[5,7,8,17–19] In fact, pre-vascularization strategies have already demonstrated to significantly reduce the time needed to vascularize the implant when compared with approaches that depend on scaffold design and delivery of angiogenic factors. However, both works describing CS pre-vascularization consisted on the individual stacking of previously formed CS monolayers, which may hinder the assembly and stratification of heterotypic cells into complex tissues such as ductlike constructs, and the development of more rigid cell structures.[20] Additionally, such methodology can be time consuming, resulting in thin cell layers difficult to manipulate and encumber to spatially control the positioning of target cells.[21,22] To circumvent those issues, Ito and co-workers have proposed a successful methodology consisting of magnetically forcing human aortic endothelial cells (HAECs), previously labeled with magnetite cationic liposomes, to deposit and adhere to a surface containing human hepatocytes, promoting cell-cell adhesion to form a 3D construct.[1,23] More recently, Gil and co-workers have also demonstrated in a proof-of-concept study the ability to create magnetic CSs by making use of rod and sphere shapes of amino-functionalized iron oxide nanoparticles.[24]

In an attempt to develop thick, stratified and hierarchical cellular 3D vascularized constructs to fit bone TE purposes, we herein propose the construction of magnetic responsive heterotypic CS by making use of iron oxide nanoparticles in a concept named magnetic force-based TE (Mag-TE). For this purpose, magnetically labeled adipose-derived stromal cells (ASCs) and human umbilical vein endothelial cells (HUVECs) were organized in a triple sheet conformation with HUVECs in between two sheets of ASCs. By forcing both heterotypic and homotypic cell-cell interactions we attempt to construct thicker and fully functional tissues. These tissues will be able to interact in a synergic trend, easing viability and proliferation as well as the secretion of growth factors and proteins that trigger both osteo- and angiogenesis in the developed tissue construct. Moreover, the sequential deposition of cells enables the accelerated development of a stratified tissue in a one-pot methodology. We therefore hypothesized that our pre-vascularized magnetically labeled CS could orchestrate the right signals towards new bone formation without requiring the supplementation of main osteogenic differentiation factors, such as dexamethasone, ascorbic acid and β-glycerophosphate; and exhibit angiogenic potential both *in vitro* and *in vivo*. The methodology herein used to create pre-vascularized and stratified cell-dense tissue opens new insights for the fabrication and repositioning of complex and higher ordered 3D connected tissue that better resembles the native *in vivo* environment.

2. Materials and Methods

All chemicals were purchased from Sigma-Aldrich and used as received, unless otherwise specified.

2.1. Synthesis and characterization of magnetic nanoparticles

Magnetite nanoparticles (MNPs) were synthesized based on the procedure previously published procedure.[24] Briefly, Fe_3O_4 MNPs were synthesized by the co-precipitation reaction of ferrous ($FeCl_2 .4H_2O$) and ferric ($FeCl_3 .6H_2O$) salts in the presence of ammonium hydroxide (NH_4OH), at 60°C and under a nitrogen atmosphere. Afterwards, MNPs' surface was modified with (3-aminopropyl)triethoxysilane (APTES) through a silanization reaction and then washed with deionized water and ethanol. Consequently, MNPs-APTES were conjugated with rhodamine B isothiocyanate (RodB) (MNPs-RodB). MNPs-APTES (previously freeze dried) were dispersed in ethanol (5 mg/mL) and then RodB (2.5 mg/mL) was added and stirred overnight at RT. Lastly, MNPs-RodB were washed until no traces of RodB were detected and freeze dried. MNPs, MNPs-APTES and MNPs-RodB were visualized by TEM (20kV, HR-TEM20-SE, JEOL), which were previously added dropwise to a carbon film copper grid and. Then, the images were analyzed by Image J software. The successful modification of the particles with APTES was confirmed by attenuated total reflectance (ATR-FTIR) by using a Bruker Tensor 27 spectrometer. The spectra were recorded at a 4 cm^{-1} resolution with a total of 256 scans in the spectral width of 4000-350 cm^{-1}.

2.2. Cell culture and cellular uptake

The collected umbilical cord was obtained under a cooperation agreement between the Aveiro Institute of Materials, University of Aveiro and Hospital do Baixo Vouga (Aveiro, Portugal), after approval of the Competent Ethics Committee (CEC). The human tissues received were handled in accordance with the guidelines approved by the CEC. Informed consent was obtained from all subjects. HUVECs were isolated following well-established protocols in the group. The enzymatic mixture containing dispase II (Sigma-Aldrich) and collagenase type IV (Sigma-Aldrich) was used for the isolation of HUVECs from cord vein. Cord vein was filled with the enzyme cocktail along the multiple site injection of enzyme cocktail in cord matrix. Afterward, the cord was incubated at 37ºC for 20 min and then, HUVECs were seeded in M199 growth medium and incubated in humidified atmosphere of 5% CO_2 at 37ºC. At the end of 4-6h, the medium was changed to M199 containing 20% umbilical cord blood serum (UCBS), 2mM L-glutamine, 5 ng/mL vascular endothelial growth factor, 10 µg/mL heparin, 100 U/mL penicillin and 100 µg/mL streptomycin.[25,26]

Human ASCs (ATCC® PCS-500-011™) were cultured in α-MEM (minimum essential medium, ThermoFisher Scientific), supplemented with 10 % of heat-inactivated FBS (Fetal bovine serum, ThermoFisher Scientific), 100 U/mL of penicillin and 0.1 mg/mL of streptomycin (ThermoFisher Scientific).

The co-location of MNPs-RodB in both HUVECs and ASCs was assessed by seeding both types of cells in well plates at cell densities of 2.4 x 10^6 cells/cm^2 for ASCs and 1.2 x 10^6 cells/cm^2 for HUVECs. Cells were cultured for 24 h at 37 °C and 5% CO_2, followed by a 4-hour incubation with MNPs-RodB at 1mg/mL. Afterwards, cells were retrieved by enzymatic digestion with trypLE Express. The cell suspension of HUVECs was immunostained with APC anti-human CD31 Antibody (5µL) (Biolegend), whereas the cell suspension of ASCs was immunostained with APC anti-human CD90 Antibody (5µL) (Biolegend) for 45 min. Both samples were washed with a staining washing buffer (2% w/v BSA, 0.1% w/v sodium citrate in PBS) and centrifuged at 500g for 5 min, followed by a resuspension in the acquisition buffer (1% v/v formaldehyde and 0.1% w/v sodium azide in PBS). The double positive cells for the pair CD31 and MNPs-RodB, and the pair CD90 and MNPs-RodB were sorted using a Cell Sorter (BD Accuri C6 Plus).

Cellular uptake was also verified using fluorescent microscopy *a priori* the formation of CSs. For this purpose, ASCs and HUVECs were seeded at the same cellular density previously mentioned

and upon 24 hours of incubation at 37 °C and 5% CO_2, MNPs-RodB (1 mg/mL), were added. After 4h cells were washed with PBS and fixed at RT in formalin (10% v/v) for 15 min. Subsequently, cells were incubated with 0.1% (v/v) Triton X100 in dPBS at RT for 5 min and incubated with Flash Phalloidin Green 488 (1:100 in dPBS) during 45 min at RT and then counterstaining with DAPI (1:1000 in dPBS) for 5 min at RT. Fluorescence microscopy analysis was performed using Axio Imager M2 widefield microscope (Carl Zeiss Microscopy GmbH) and using ZEN v2.3 blue edition.

2.3. Development of homotypic and heterotypic magnetic CS

To achieve a heterotypic CS, ASCs and HUVECs were organized in a stratified triple sheet conformation with the endothelial cells layered in between the two sheets of ASCs. For the purpose, ASCs were seeded at density of 2.4 x 10^6 cells/cm^2. After 24 h of incubation at 37 °C and 5% CO_2, MNPs-RodB (1 mg/mL), were added. After 4h, cells were detached by adding trypLE Express followed by a 5 min incubation at 37 °C. Cells were then centrifuged at 300 g and then, the magnetically labeled cells were transferred to ultralow-attachment 24, 48 or 96-well plates (previously treated with 2%, w/v alginate solution during 30 min). Commercial neodymium rod magnets Ø 10 mm, height 40 mm (strength of 108N and standard N41 magnetization) (Supermagnet) were placed at the bottom of the reverse side of the ultralow-attachment plate to provide magnetic force to the plate, during the timeframe of the culture. After 24h, the magnetically labeled HUVECs were added at a density of 1.2 x 10^6 cells/cm^2 on top of the previously established ASCs monolayer. Lastly, 2.4 x 10^6 cells/cm^2 of magnetic labeled ASCs were added (24h after HUVECs magnetic deposition) and the final structure with a triple sheet conformation was cultured for 7, 14 and 21 days. Homotypic CS were used as control and were produced following the same above-mentioned methodology but omitting the addition of HUVECs. A second ASCs layer was added to the ASCs monolayer after 24h. Homotypic CS were also cultured during 7, 14 and 21 days. Both homotypic and heterotypic CSs were cultured in M199 medium supplement with heparin and ECGS with or without osteogenic differentiation factors, namely dexamethasone (10nM), ascorbic acid (50μg/mL) and β-glycerophosphate (10mM).

2.4. CS characterization

Heterotypic and homotypic CSs cultured for 7 days in basal conditions (no osteogenic factors), were fixed in formalin 10% (v/v) during 15 min at RT. Then, the CSs were permeabilized with 0.1 (v/v) Triton X for 5 min at RT. Afterwards, CSs were immersed in 5 % (v/v) FBS/dPBS for 1h at RT and then incubated with the anti-rabbit human vinculin antibody (1:50 in 5% FBS/dPBS, Invitrogen) for 3h at RT. After washing the samples with PBS, the CSs were incubated with the secondary antibody donkey anti-rabbit AlexaFluor 594 (1:400 in 5% FBS/dPBS). To confirm the presence of HUVECs in the developed heterotypic CSs, a similar immunofluorescence procedure was performed with the addition of the mouse anti-human CD31 (1:50 in 5% FBS/dPBS, BioLegend) conjugated with the secondary antibody goat anti-mouse AlexaFluor 647 (1:400 in 5% FBS/dPBS). The CSs were incubated with Flash Phalloidin Green 488 (1:100 in dPBS) during 45 min at RT and then counterstaining with DAPI (1:1000 in dPBS) for 5 min at RT. Finally, the samples were analyzed by confocal microscopy (LSM 880, ZEISS). The morphology of both homotypic and heterotypic CSs cultured for 7, 14 and 21 days under basal and osteogenic media was also accessed by Scanning Electron Microscopy (SEM). For the purpose, samples were washed with PBS and fixed at RT in formalin (10% v/v) for 15 min. After 1 h, samples were dehydrated in an increasing gradient series of ethanol for 10 min each. The

samples were gold sputter-coated using an accelerating voltage of 25 kV and visualized by SEM (S4100, Hitachi, Japan).

2.5. Mitochondrial metabolic activity quantification

Mitochondrial metabolic activity was determined using a MTS colorimetric assay (CellTiter96® AQueous one solution cell proliferation assay, Promega) in agreement to manufacture's specifications. CSs (n=3) were incubated with the reagent kit (120 µl per well) and incubated at 37 °C during 4 h, protected from light. Lastly, the absorbance was read at 490 nm using a microplate reader (Synergy HTX, BioTek Intruments, USA).

2.6. Cell proliferation quantification

Total DNA quantification of the CSs (previously cultured during 7, 14 and 21 days) was performed after cell lysis (Quant-iT™ PicoGreen™ dsDNA Assay Kit, Invitrogen™). CSs (n=3) were suspended in ultra-pure sterile water with 2 % (v/v) Triton 100X during 1 h at 37 °C and then the samples were frozen at −80 °C and stored until further use. Samples were defrosted and used according to the specifications of the kit. MNPs-RodB were magnetically segregated using a neodymium magnet to assure that only DNA content would be selected for the quantification assay. A standard curve for DNA analysis was generated with the provided DNA standard from the DNA assay kit. After 10 min of incubation at RT, fluorescence was read at an excitation wavelength of 485/20 nm and 528/20 nm of emission using a microplate reader (Synergy HTX, BioTek Intruments, USA).

2.7. Cell viability

The survival of the developed CSs was evaluated by a live-dead fluorescence assay according to the manufacturer's recommendation (ThermoFisher Scientific). On days 7, 14, or 21, samples were washed with PBS and then stained with the kit components at 37ºC for 20 min and protected from light. Afterwards, samples were visualized by fluorescence microscopy (Axio Imager 2, Zeiss).

2.8. Analysis of osteogenic differentiation of CS

The ability of HUVECs to induce osteogenic differentiation over ASCs was evaluated in growth medium with and without osteogenic differentiation factor. Homotypic CSs with ACSs were used as control. All CSs were incubated for 7, 14 and 21 days.

2.9. ALP activity measurement assays

After each time point, the CSs were lysed by the same procedure in the section of cell proliferation quantification. ALP activity was determined in the lysates by using 4NPhP ALP-mediated hydrolysis to quantify 4NPh release. 25 µL of each lysate sample was added to 75 µL of a freshly prepared 4NPhP solution (2 mg/mL) in 1M diethanolamine (DEA) buffer (pH 9.8, with 0.5×10^{-3}M $MgCl_2$). Samples were incubated in the dark at 37 °C for 45 minutes. Enzymatic activity was then quantified by UV–vis 405 nm (Synergy HTX, BioTek Intruments, USA). The value was normalized against the previously determined correspondent DNA concentration (µg/mL). A standard curve of 4NPh was used as reference (0, 15×10^{-6}, 30×10^{-6}, 50×10^{-6}, 75×10^{-6}, 95×10^{-6} M in DEA buffer).

2.10. Osteopontin immunostaining

Prior to cell seeding, ASCs and HUVECs were incubated with the lipophilic dyes 3,3′-dioctadecyloxacarbocyanine perchlorate (DIO, green) and 1,1'-Dioctadecyl-3,3,3',3'-

Tetramethylindodicarbocyanine (DID, purple), respectively. Cells were incubated with each dye (1mL, 2μM per 1× 10^6 cells) at 37 °C for 30 min, as described by the manufacturer. The expression of osteopontin on the CSs was visualized by fluorescence microscopy. At each time point, the samples were washed with PBS and fixed at RT in formalin (10% v/v) for 15 min. Initially, CSs were incubated with 0.1% (v/v) Triton X100 in dPBS at RT for 5 min. Subsequently, the samples were rinsed and incubated in 5% (v/v) FBS/dPBS solution during 1h at RT. Afterwards, CSs were washed and incubated with 400 µl of mouse anti-human osteopontin antibody (1:100 in 5% FBS/dPBS, Biolegend, Taper) during 3h at RT. Then, the samples were incubated with the anti-mouse Alexa Fluor 555 conjugated dye solution (1:400 in 5% FBS/dPBS) for 1h in dark at RT. Lastly, the CSs were incubated with 400 µl of DAPI solution to nuclei staining (1:1000 in dPBS) during 5 min in the dark at RT. Homotypic CSs were used as control. Fluorescence microscopy analysis were performed in Axio Imager M2 widefield microscope (Carl Zeiss Microscopy GmbH) and using ZEN v2.3 blue edition.

2.11. ELISA immunoassay quantification of cytokines

The expression of osteopontin and osteocalcin was determined through Human Osteopontin and Osteocalcin ELISA Kits (Abcam), respectively according to the manufacturer's instructions. Human bone morphogenic protein-2 (BMP-2) and vascular endothelium growth factor (VEGF) were also quantified using BMP-2 (Invitrogen) and VEGF (Abcam) ELISA Kits, and used according manufacture's specifications. Culture media from the MTS, DNA and ALP activity assays over 21 days were collected and stored at -80ºC until further use. The absorbance was then read at 450 nm using a microplate reader (Synergy HTX, BioTek Intruments, USA) (21 days for osteopontin and osteocalcin and 7,14, 21 for BMP-2 and VEGF).

2.12. Analysis of biomineralization of the CS

In vitro mineralization of CSs was accessed at 7, 14 and 21 days of culture in medium with or without osteogenic differentiation factors. Firstly, the CSs were fixed at RT in formalin (10% v/v) for 15 min. Posteriorly the OsteoImage™ Assay was used to visualize the hydroxyapatite portion of bone-like nodules deposited by cells. The OsteoImage™ Staining reagent (1:100 v/v) was added to the previously fixed CSs and incubated for 30 min. After this, the CSs were washed 3 times and visualized under fluorescence microscope. The mineral formation was also accessed using SEM. Energy dispersive X-ray spectroscopy (EDS) (QUANTAX 400, Bruker) was used to examine the chemical composition of the mineral's deposits within the CS. The samples were carbon-coated and imaged at an electron in intensity of 15 kV (SU-70, Hitachi). The immunofluorescence staining in the histological sections was also performed for the heterotypic CSs at 21 days cultured with or without osteogenic differentiation factors. The samples were previously fixed with 10% (v/v) and then, CSs were routinely processed in an automated system and embedded in paraffin. Afterwards, sequential sections of 5 µm thickness were made in adhesive slides for Von Kossa and Masson's Trichrome staining. The percentage of collagen matrix and number of Ca deposits in the histological cuts were analyzed using Image J software.

2.13. Assessment of *in vivo* angiogenic potential using a chick embryo model

2.13.1. Implantation in chick chorioallantoic membrane (CAM) and neo-vessel quantification

The angiogenic potential of the heterotypic CS (previously cultured in basal media for 7 days) was evaluated using the chick embryo CAM assay. Fertilized chick (Gallus gallus) eggs were incubated horizontally at 37.8 °C in a humidified atmosphere and referred to as embryonic day

(E). On E3, 1.5–2 mL of albumin was removed to allow the detachment of the developing CAM and a square window was opened in the shell. This window was sealed with a transparent adhesive tape and the eggs returned to the incubator. On E10, a 3-mm silicon ring was placed on top of the CAM and filled with CSs under sterile conditions. Basic fibroblast growth factor (bFGF) and PBS were used as positive and negative controls, respectively. Eggs were re-sealed and returned to the incubator for 4 days, being hydrated every day. Embryos were euthanized by adding fixative (2 mL) on top of the CAM, the ring was removed, and the CAM was excised. The inoculation area (CAM host controls and CAM with the CS) was photographed *ex ovo* under a stereoscope, at 20x magnification (Olympus, SZX16 coupled with a DP71 camera). The number of new/recruited vessels (less than 20 μm diameter) growing radial towards the ring area was counted in a blind fashion. All experiments were carried out according to the European Directive 2010/63/EU and the national Decreto-Lei nº113/2013.

2.13.2. Image analysis: quantification of the total number of vessels and junctions

For a quantitative analysis of the total number of vessels and junctions, CAM images were treated using ImageJ, by adapting a described methodology[27] for vessel and capillary skeletonization. "FeatureJ Laplacian" plug-in was replaced by a "Mexican Hat" plug-in with a radius of 3, due to a greater adaptability to the samples, and a threshold of 1-130 was set prior to skeletonization (plug-in "Skeletonize 2D/3D"). Image skeletonization was restricted to the ROI. The number of junctions (vascular ramifications) and total number of vessels was calculated using the ImageJ plug-in "Analyse Skeleton 2D/3D" (n=3).

2.14. Histological and immunohistochemical analysis of individual CSs and CAM with CS

Samples of CS and CAM with CS were paraffin-embedded and 5-μm cross-sections were obtained from 2 to 3 standardized transversal planes using a Thermo Scientific HM550 microtome. Sections were stained with H&E and images were obtained using the Axio Imager M2 widefield microscope (Carl Zeiss Microscopy GmbH).

Expression of von Willebrand factor (VWF)/fibronectic (FN), CD31/collagen type IV, VWF/CD31 (all for CS) and VWF/human nuclei (HuNu) (for CAM with CS) was probed after antigen recovery. For this, masked epitopes were exposed by treatment with TE buffer (10 mM Tris/1 mM EDTA, pH 9) for 35 min at 95–98 °C. Sections were incubated with rabbit anti-VWF (1:400 in 5% FBS/dPBS, Abcam) and FN monoclonal antibody (FN-3) Alexa Fluor 488 (1:100, Thermofisher), with mouse anti-human CD31 (1:50 in 5% FBS/dPBS,BioLegend) and rabbit anti-collagen IV (1:400 in 5% FBS/dPBS, Abcam), and mouse anti-human nuclei (1:400, Abcam) primary antibodies. This was followed by 1 h–incubation with Alexa Fluor 647-labeled chicken anti-rabbit (1:400 in 5% FBS/dPBS, Invitrogen) (VWF), AlexaFluor 488 Goat anti- mouse (1:400 in 5% FBS/dPBS, Invitrogen) (CD31 and HuNu) and AlexaFluor 594-labeled donkey anti-rabbit (collagen IV). All sections were counterstained with DAPI (Sigma). Control sections for each immunolabelling excluded primary antibody staining were performed. Images were obtained using a fluorescence inverted microscope (AxioImager Z1, Zeiss).

2.15. Statistical analysis

Statistical analysis was performed using GraphPad Prism software (GraphPad Software Inc., version 7.0) with two-way ANOVA following the Bonferroni post hoc test, with a significance level at $p < 0.05$: *$p < 0.05$; **$p < 0.01$; *** $p< 0.001$; ****$p < 0.0001$.

3. Results

3.1. MNPs characterization

Continuous homotypic and heterotypic magnetic CSs were prepared via Mag-TE. For this purpose, MNPs were synthetized as described in Fig. S1A. Upon characterization via TEM, it was determined that MNPs presented sizes ranging from 5-15nm (Fig.S1B). Subsequently, MNPs were amino-functionalized as previously described,[24] and such modification was confirmed through FTIR-ATR. The characteristic bands of MNPs associated with the Fe-O vibration were evidenced below 700 cm^{-1} (Fig.S1C-i).[28] The characteristic band at 1634 cm^{-1} was associated with the N-H bend in primary amines, which may be correlated with the fabrication method employed (using ammonium hydroxide). The functionalization of MNPs with APTES (Fig.S1C-ii) caused slight deviations from the characteristic bands below 700 cm^{-1}. Further characteristic bands appeared on the APTES modified MNPs. Specifically, the absorption band at 993 cm^{-1} was associated with Fe-O-Si vibration, the low-intensity bands in the 1300–1600 cm^{-1} range are attributed to the amino-propyl segment and free amino groups and the bands in the range 2853-2954 cm^{-1} match the vibration of the CH_2 group.[28] The modification of MNPs-APTES with RodB was also confirmed by FTIR-ATR (Fig.S1C-iii). Upon the incorporation of RodB (Fig.S1C-iv), the carboxylic groups of the compound, represented by the C=O characteristic band at 1709 cm^{-1}, undergo esterification causing a shift in the C=O vibration. Moreover, the incorporation of RodB caused a shift in the Fe-O-Si characteristic band evidenced in APTES-MNPs (993- 1007 cm^{-1}). A new low intensity peak appeared at 1222 cm^{-1} and was associated with C-H in plane bend. The characteristic peak evidenced in the whole spectra at approximately 3400 cm^{-1} was attributed to the O-H vibration.[29]

3.2. CS fabrication, 3D stratification and their characterization

The successful isolation of HUVECs from umbilical cord was determined by flow cytometry (Fig.S2). More than 98% of HUVECs revealed positive markers for CD31.

Prior to CS formation, MNPs-RodB were successfully uptaken by HUVECs (81.4 ± 1.5%) and ASCs (93.1± 4.6%), as corroborated in Fig.1A and B.

Homotypic CSs comprising of two ASCs and heterotypic CSs composed of two ASCs layers with one CS of HUVECs in between, were produced following the methodology represented in Fig.1C. As previously described by Ito and co-workers, the thickness of individual CS was controlled by manipulating the amount of cells in suspension and the area of the well plate.[1,20,30]

CD31 immunodetection highlighted the presence of HUVECs in the middle of the fabricated CS (Fig. 2A) where, via vinculin staining, it was possible to attest the existence of cell-cell adhesions throughout the developed construct (Fig. S3). 3D reconstruction and different side views (top and middle) are displayed in Fig.2B. The integrity of the vascularized CS membrane was corroborated by SEM (Fig. 2C). Moreover, tubular-like structures (represented in red), were evidenced in between two ASCs layers, displayed in green.

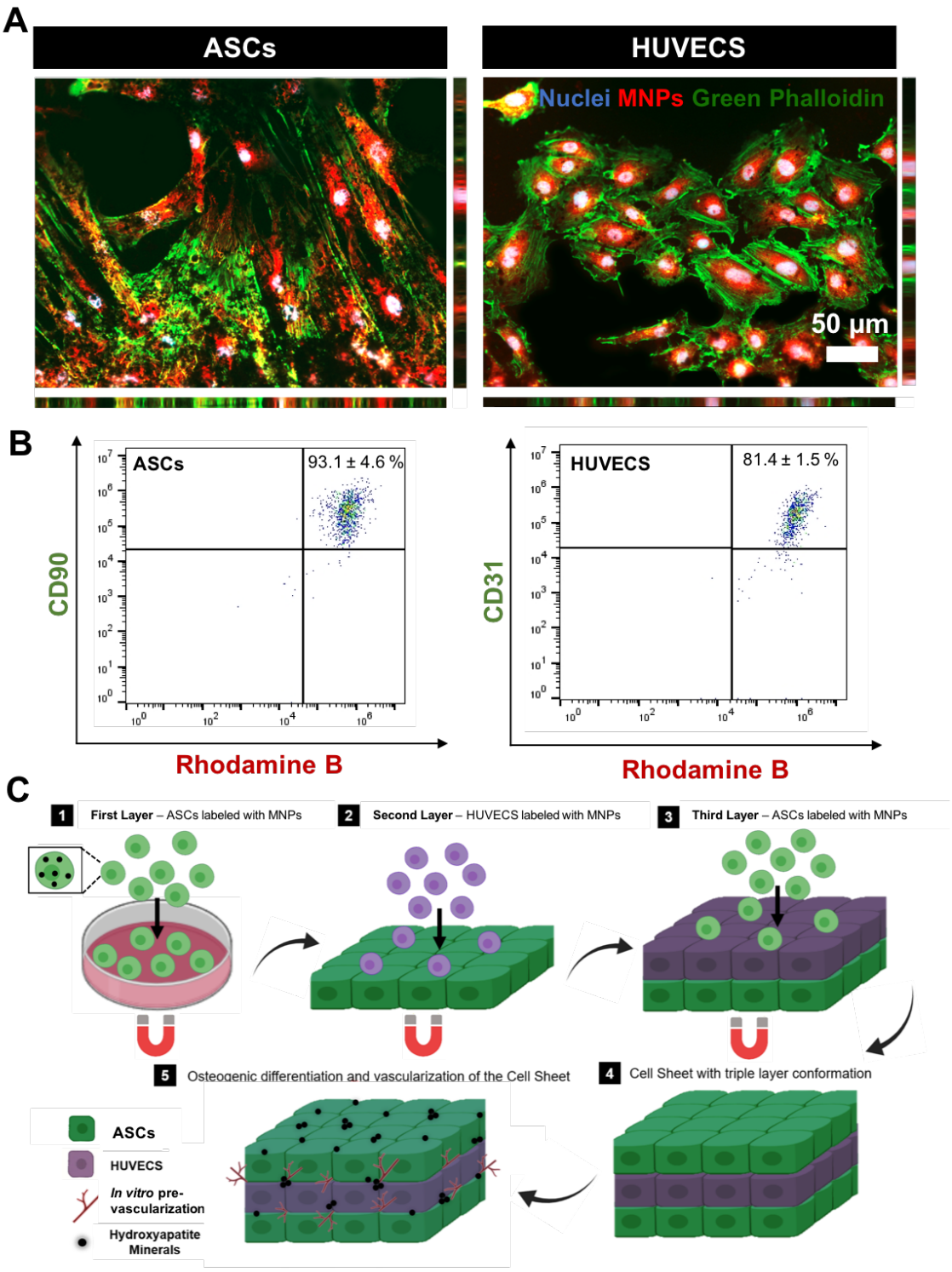

Fig.1. Cellular uptake and graphical illustration of the CS fabrication. (**A**) Internalization of MNPs-RodB in ASCs and HUVECs: actin filaments of HUVECs and ASCs (green phalloidin), MNPs-RodB (red) and cell nucleus - DAPI (blue). (**B**) Flow cytometry analysis of MNPs-RodB uptake after 4 hours. (**C**) Schematic representation of the fabricated 3D vascularized heterotypic CS.

3.3. Metabolic activity and cell proliferation and survival

Homotypic and heterotypic CS in both basal and osteogenic medium showed an increased metabolic activity (Fig. 2D) and DNA (Fig. 2E) content up to 14 days of culture. Live-dead assay showed that up to 21 days post-CSs' formation, the majority of the cells remained viable for all formulations (Fig. 2F and Fig.S4). Notably, these results also evidenced the ability of CSs for long-term cell survival, which is a major challenge in tissue engineering strategies aiming CSs fabrication.

3.4. *In vitro* assessment of the osteogenic potential of the Mag-TE Cell sheets:

3.4.1. Quantification of the ALP activity and mineralization assessment

Based on the knowledge that increased levels of ALP activity are correlated with enhanced osteogenic differentiation, it is possible to assure that cell differentiation had occurred earlier (7 days) for the heterotypic CS cultured with osteogenic media (Fig.2G). However, at the end of 21 days both heterotypic CS cultured in either basal or osteogenic media, showed enhanced ALP activity, corroborating the fact that ASCs co-cultured with HUVECs lead to an enhanced cell differentiation, although delayed (7 days) when compared with the heterotypic CS cultured in osteogenic media. As expected, the ACSs monolayer cultured under osteogenic conditions revealed some ALP increment after the 21 days, as the ACSs monolayer in basal conditions did not show any ALP increment over time.

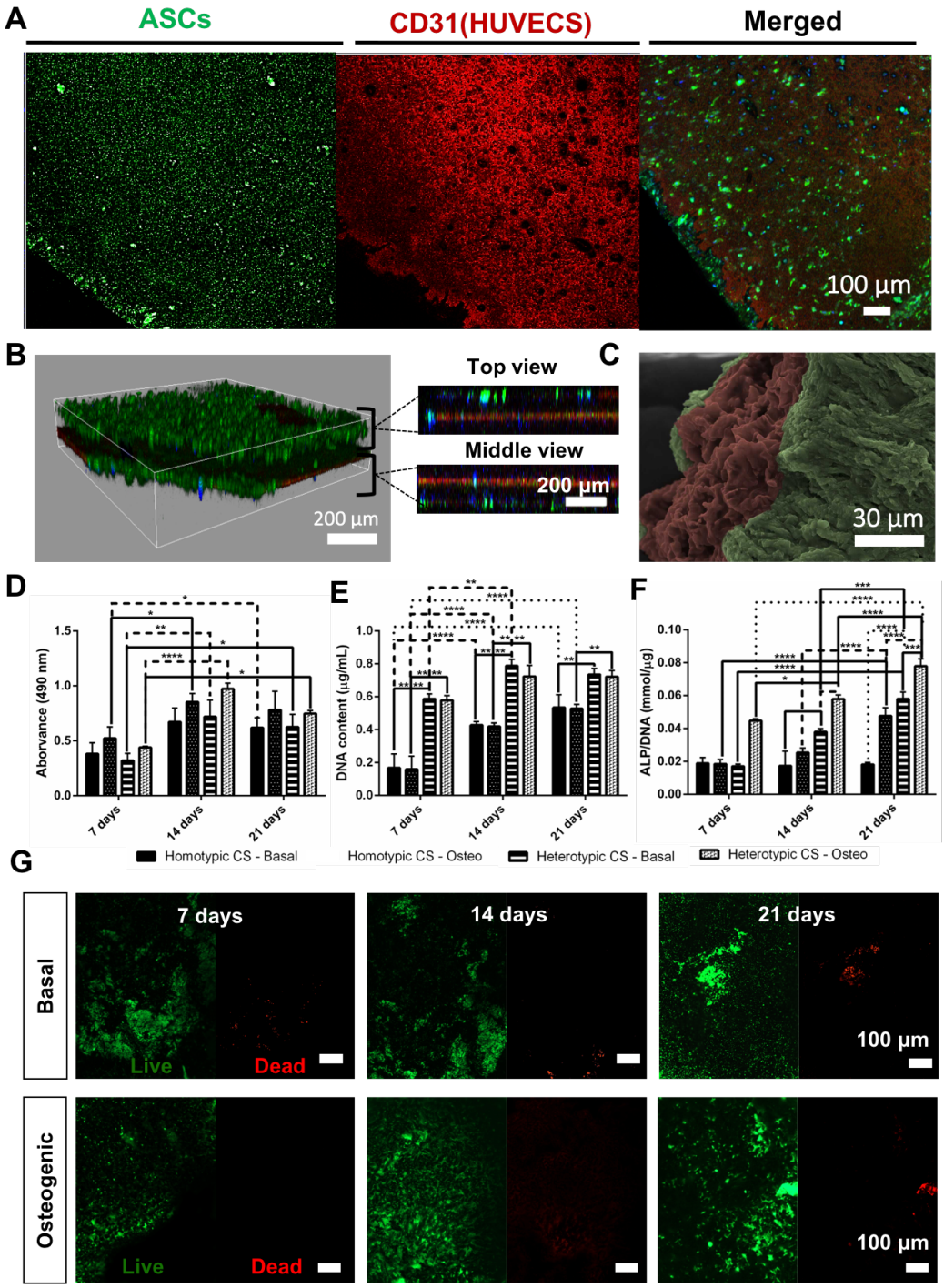

Fig.2. Cell sheet integrity, metabolic activity, cell survival and proliferation, and *in vitro* osteogenic potential. (A) Confocal microscopy of the magnetically labeled CS demonstrating CD31 staining HUVECs in between two ASCs sheets – CD31: HUVECs (red) and ASCs (green); **(B)** 3D reconstruction of B and side sections exhibiting CD31 (HUVECs) in the middle of two ASCs sheets (Phalloidin – green, DAPI – blue). (**C**) SEM micrographs of the triple layer conformation of the developed CS: HUVECs (represented in red) and ASCs (represented in green). **(D)** Cell metabolic activity determined by MTS colorimetric assay, **(E)** Cell proliferation by DNA quantification and **(F)** Alkaline phosphatase (ALP) activity normalized by DNA content for both homotypic and heterotypic CS. All results were significantly different unless marked with ns ($p > 0.05$). **(G)** Live-dead fluorescence assay at day 7, 14 and 21 of culture in basal and osteogenic medium. Living cells were stained by calcein (green) and dead cells by propidium iodide (red).

The mineralization of the heterotypic CSs was also evidenced by EDS and Osteoimage™ assay and the results support the ALP findings. Hydroxyapatite crystals were also evidenced in both culturing conditions after 14 days (Fig. 3A). The chemical analysis of the minerals by EDS displayed calcium (Ca) and phosphate (P) peaks increasing over time in both basal and osteogenic conditions, with a higher Ca/P ratio attained for the heterotypic CS cultured for 21 days under osteogenic media (Fig.3B). The ratio between Ca/P achieved for the heterotypic CSs cultured in basal conditions re-suggests a delayed (7 days) osteogenic differentiation. The enhanced deposition of hydroxyapatite-like minerals evidenced in both conditions with the ratio of Ca/P approaching the one of the apatite minerals in bone (*1.66),[31,32] indicates the formation of bone-like tissue for the heterotypic CS, even in the absence of osteogenic factors. Nevertheless, no significant differences were evidenced. In addition, the decline in iron (Fe) detection overtime was in agreement with cell proliferation and *de novo* matrix formation that leads to a decrease signal.

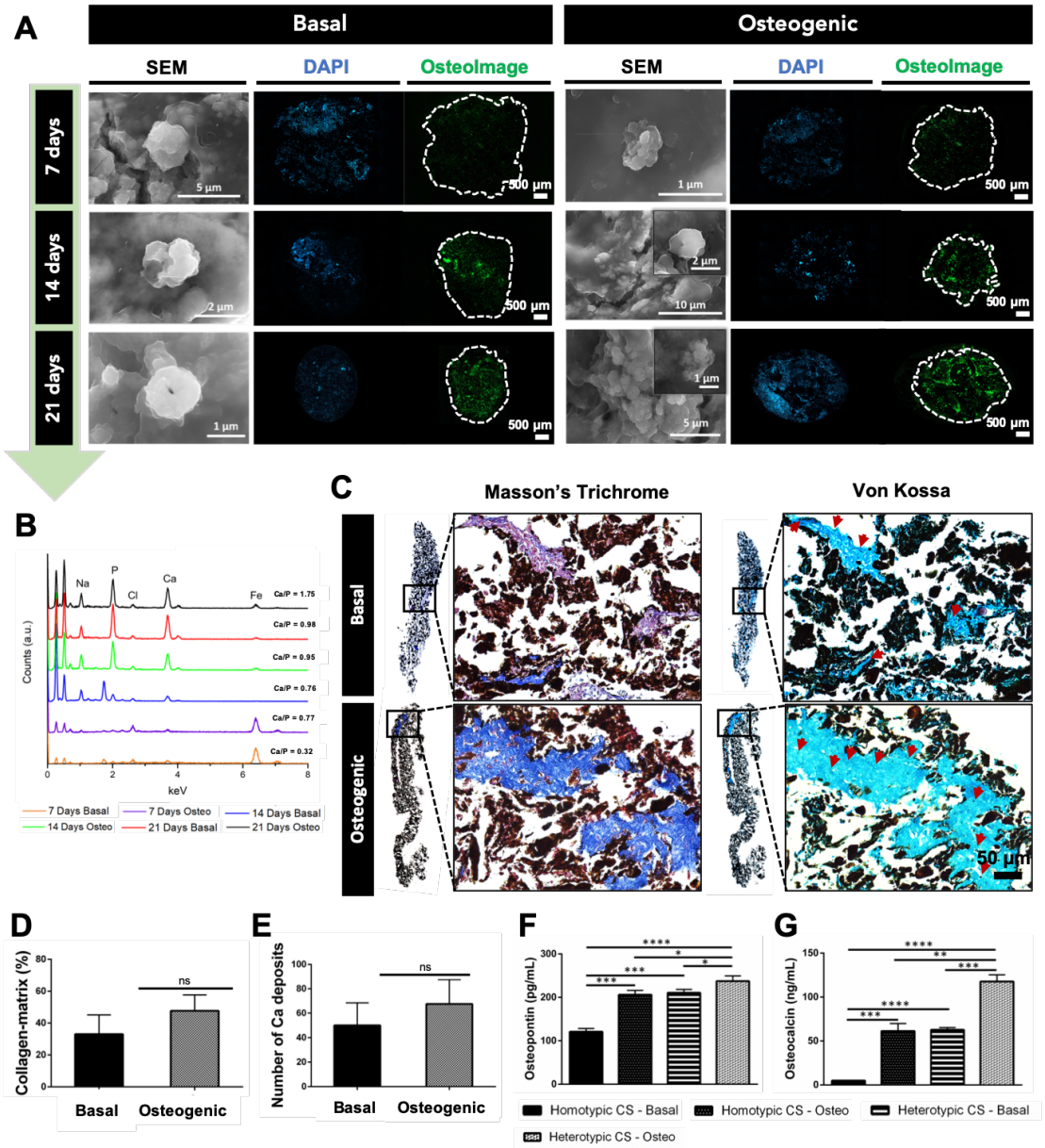

Fig.3. Mineralization of the developed 3D heterotypic CS in basal and osteogenic media. (**A**) The hydroxyapatite portion of bone-like nodules deposited by cells was visualized through fluorescent

OsteoImage™ Mineralization Assay: cell nucleus - DAPI (blue) and hydroxyapatite (green). SEM micrographs displaying calcium deposits are depicted in the right panel; (**B**) Energy dispersive X-ray spectroscopy (EDS) spectra of minerals formed within the CS; (**C**) mineralization of the heterotypic CS accessed by Von Kossa staining and collagenous connective tissue fibers identified by Trichrome Masson staining on histological sections CS cultured in basal or osteogenic media after 21 days. (**D**) Percentage of collagen-matrix in the representative histological cut; (**E**) Number of Ca deposits in the *de novo* cell matrix; **(F)** Quantification of osteopontin and osteocalcin expression by **(G)** ELISA). $p < 0.05$: *$p < 0.05$; **$p < 0.01$; ***$p < 0.001$; ****$p < 0.0001$.

Furthermore, Von Kossa staining revealed the presence of Ca deposits within the *de novo* matrix formed, and Masson's Trichrome technique also demonstrated a collagen enriched matrix in the developed construct (Fig. 3C, 3D and 3E).

3.4.2. Cytokines detection

The secretion of the late osteogenic markers osteopontin and osteocalcin was evidenced after 21 days in both culturing conditions in the homotypic and heterotypic CSs (Fig.3F and G, respectively). As anticipated, magnetically labeled homotypic CS in the absence of osteogenic factors secreted none (for osteocalcin) or few (for osteopontin) of the osteogenic markers. The obtained results for the release of both osteopontin and osteocalcin cytokines suggested a similar tendency between the magnetically labeled homotypic CS cultured with osteogenic factors and the heterotypic CS cultured in the absence of the osteogenic factors. Again, the results suggested an osteogenic role of HUVECs over ASCs. To further explore other forms of osteopontin presence in the magnetically labeled heterotypic CS, an immunofluorescence assay was also performed. The results, displayed in Fig. 4, demonstrated a complete osteopontin staining after 21 days in both culturing conditions. SEM micrographs were taken from every representative condition. Fig. S5, which demonstrated the immunofluorescence assay of osteopontin for homotypic CSs, also exhibited a complete osteopontin staining after 21 days in osteogenic conditions. As expected, no osteopontin staining was evidenced in the homotypic CSs under basal conditions.

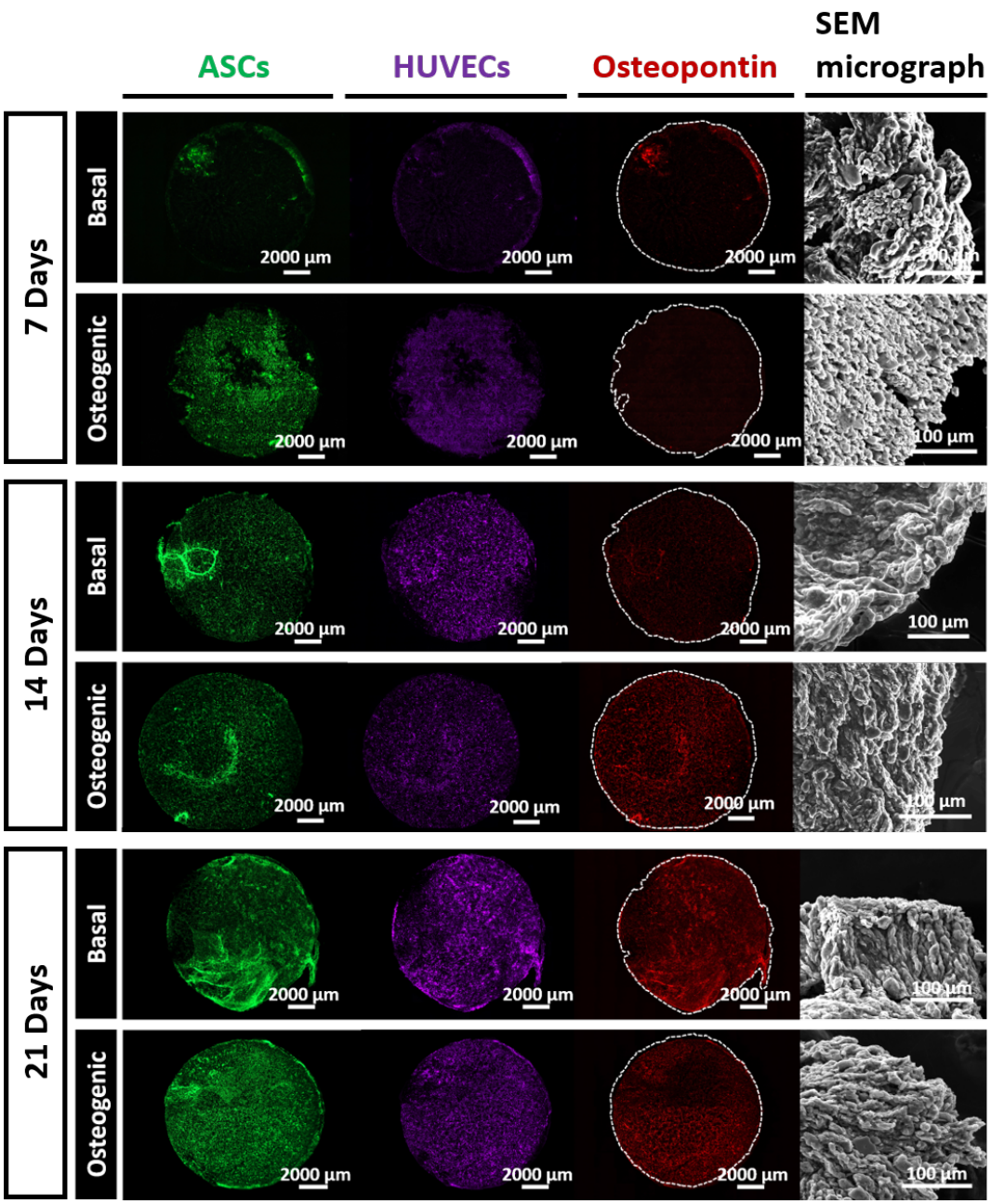

Fig. 4. Osteopontin staining and SEM micrographs of heterotypic CS. Immunofluorescence of ASCs (green), HUVECs (purple) and osteopontin (red) in 3D heterotypic CS cultured for 7, 14 and 21 days in basal and osteogenic media**.** SEM micrographs of the developed CSs are represented in the right panel demonstrating CS integrity.

The secretion of BMP-2 and VEGF was also investigated over a period of 21 days (Fig.5A,B). The results insinuate a synergic behavior between BMP-2 and VEGF. BMP-2 was found to be enhanced for the heterotypic conditions, with a more pronounced effect ($P<0.01$) on the CSs cultured with osteogenic supplements, for every single timepoint, with increased expression at 21 days. On the other hand, the highest levels of VEGF were achieved for the homotypic CS cultured in basal conditions, followed by the ones cultured in osteogenic condition, again regardless of the timepoint. The decreased VEGF values obtained for the heterotypic CS supported osteogenic differentiation. In fact ASCs stimulate blood vessel growth via the secretion of angiogenic and anti-apoptotic growth factors, such as VEGF, enhancing the biological activity of endothelial

cells.[7,13,33,34] Nevertheless, decreased levels of VEGF with enhanced values of BMP-2 suggested the osteogenic differentiation of ASCs that, once differentiation has occurred, lose their ability to enhance angiogenesis by down-regulating VEGF levels. Moreover, the effect of VEGF over endothelial cells is known to induce the release of BMP-2,[13,35,36] which is in agreement with the data herein acquired: even in the absence of osteogenic factors, BMP-2 is increased in the endothelized CS. The results insinuate the synergic interaction between the layers of ASCs and HUVECs, even in the absence of osteogenic differentiation factors, corroborating CS stratification, achieved through Mag-TE.

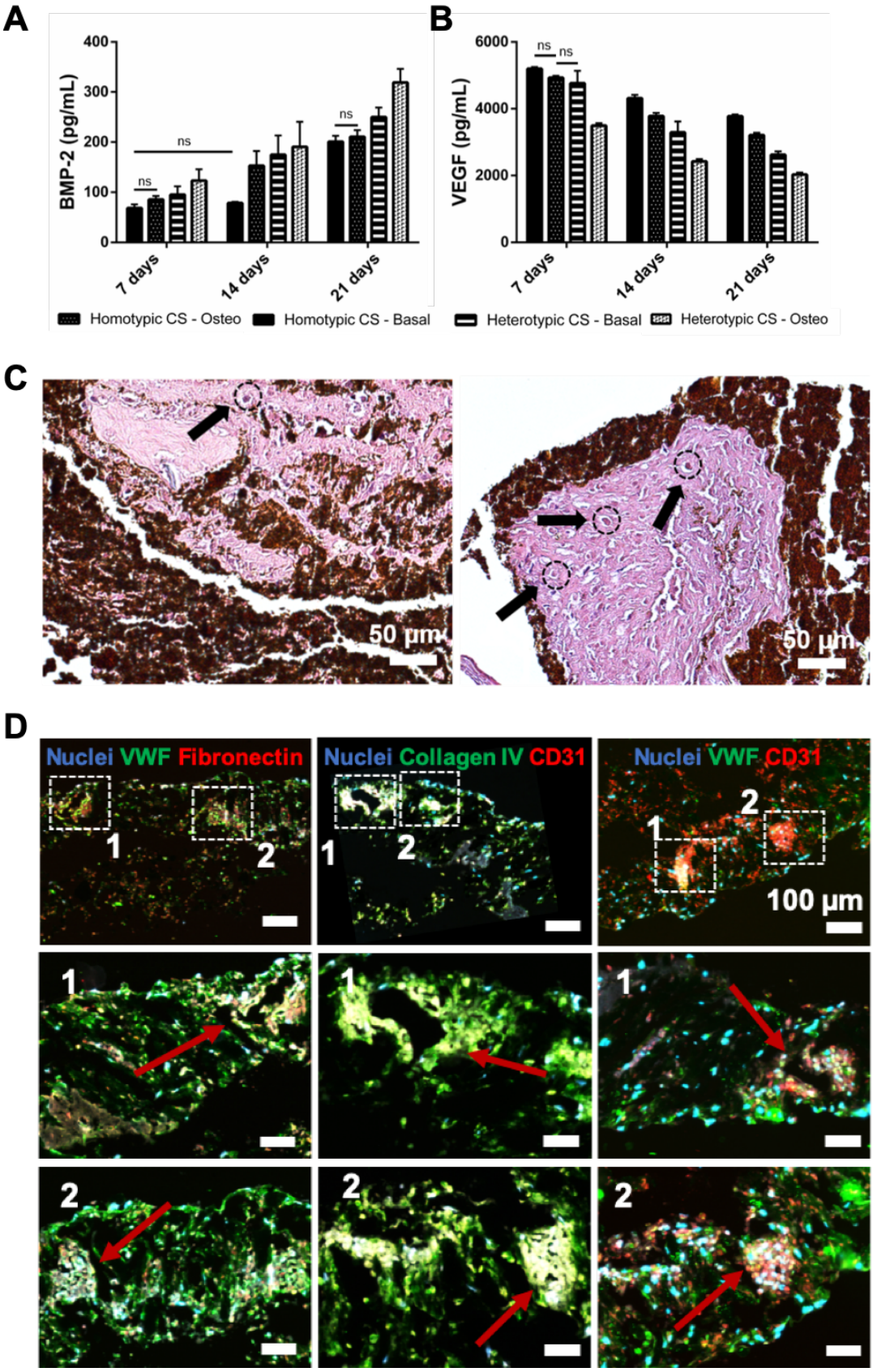

Fig.5. Pre-vascularization of the heterotypic CS cultured during 7 days with basal media. (**A**) Quantification of BMP-2 and (**B**) VEGF release by Elisa on the homotypic and heterotypic CS cultured over 21 days in basal and osteogenic media; (**C**) H&E staining of paraffin-embedded heterotypic CSs cultured under basal conditions for 21 days; (**D**) Immunostaining of CS: VWF (green) and FN (red);

collagen IV (green) and CD31 (red); and VWF (green) and CD31 (red) demonstrating the presence of capillary-like structures (white arrows). DAPI (in blue) stains all nuclei.

3.5. Angiogenic potential

De novo matrix formation and pre-vascularization of heterotypic CSs cultured under basal conditions were evidenced after 21 days of culture (Fig.5C). H&E staining of the CSs revealed the presence of tubular-like structures in the *de novo* matrix formed. To corroborate the presence of vascular structures within the CS, the sections were stained with the endothelial marker CD31 and collagen IV, a main protein component of all basement membrane that has a crucial role in endothelial cell proliferation and cell behavior.[37] VWF and FN immunostaining also exposed the presence of capillary-like structures within the CS, corroborating our findings. All sections were counterstained with DAPI to stain the cells' nuclei. For a better visual interpretation of the capillary-like structures, a VWF and CD31 immunostaining was also performed (Fig. 5D and Fig.S6)

A CAM assay was performed to evaluate the *in vivo* angiogenic potential of our magnetic heterotypic CSs cultured in basal medium. The developed CSs were harvested with the aid of a neodymium magnet and implanted inside a silicon ring placed on top of the CAM and cultured for 4 days, as represented in Fig.6A. Photomicrographs were taken to count the number of newly formed blood vessels (Fig. 6B). The results demonstrate that our endothelized CS was able to recruit new microvessels at a same extent of bFGF, used as a positive control, and significantly higher than the negative control (PBS) Fig. 6C. The total number of vessels and junctions were also quantified using ImageJ. Although higher values were verified for the heterotypic CSs in comparison with the negative and positive controls(Fig. S7), no significant differences were observed.

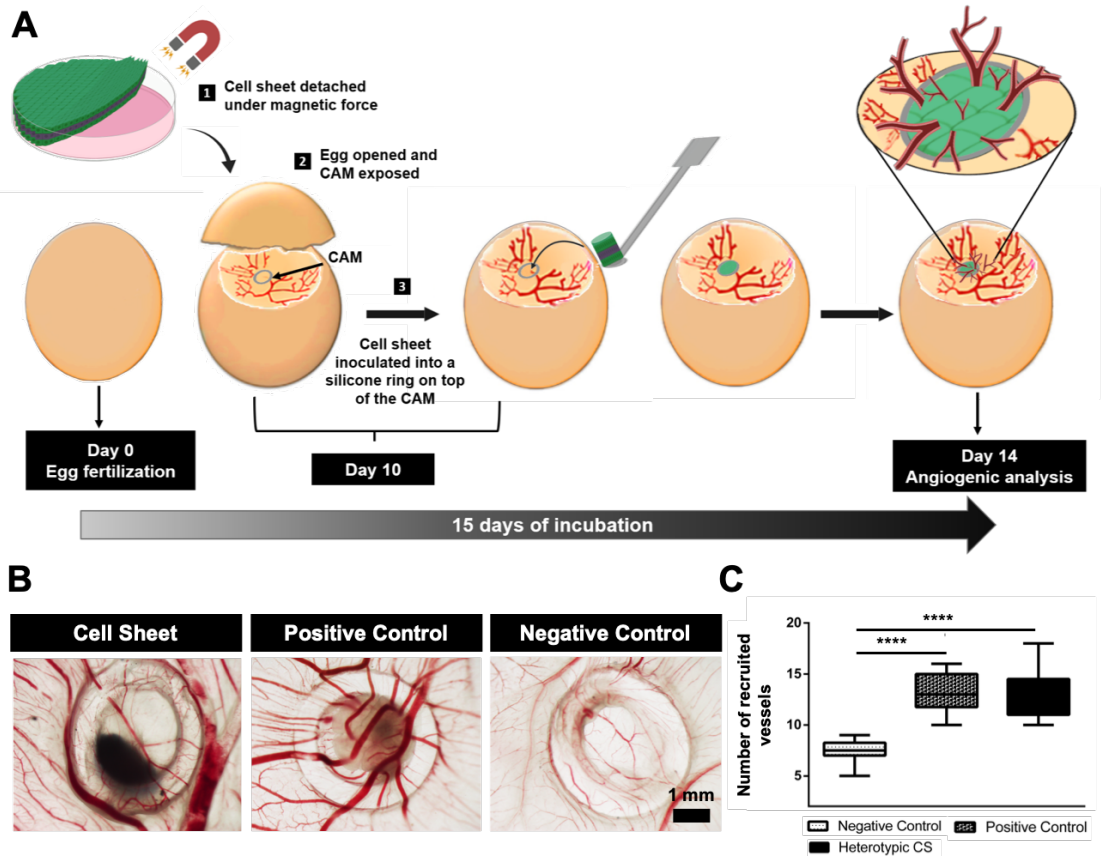

Fig.6. ***In vivo*** **angiogenic potential of the heterotypic CS cultured during 7 days with basal media.** PBS was used as negative control and bFGF as a positive control. **(A)** Schematic representation of the implementation of the CS into the CAM; (B) Photomicrographs of the newly formed vessels (C); Quantification of the newly formed vessels after 14 days of maturation (****$p < 0.0001$).

H&E staining of paraffin-embedded CAMs showed that our magnetically labeled CSs were able to incorporate into the host tissue. The appearance of MNPs within the CAM of the host supported this finding (Fig.7A). To further track the implanted human cells, the specific human nuclei marker was also used (HuNu, stained in pink). Human nuclei were found all over the host membrane corroborating the cellular invasion from the cells of our heterotypic CS (Fig.7B). Moreover, the combination of HuNu with VWF immunostaining exposed HUVECs organized in capillary-like structures within the CS tissue, as well as human cells integrating chick vasculature (zoom sections of Fig.7C). In fact, the combination of HuNu with VWF inside chick vessels lead us to conclude that human endothelial cells were in fact integrating such vascular regions (Fig. S8). The positive control (bFGF) was used to corroborate our findings.

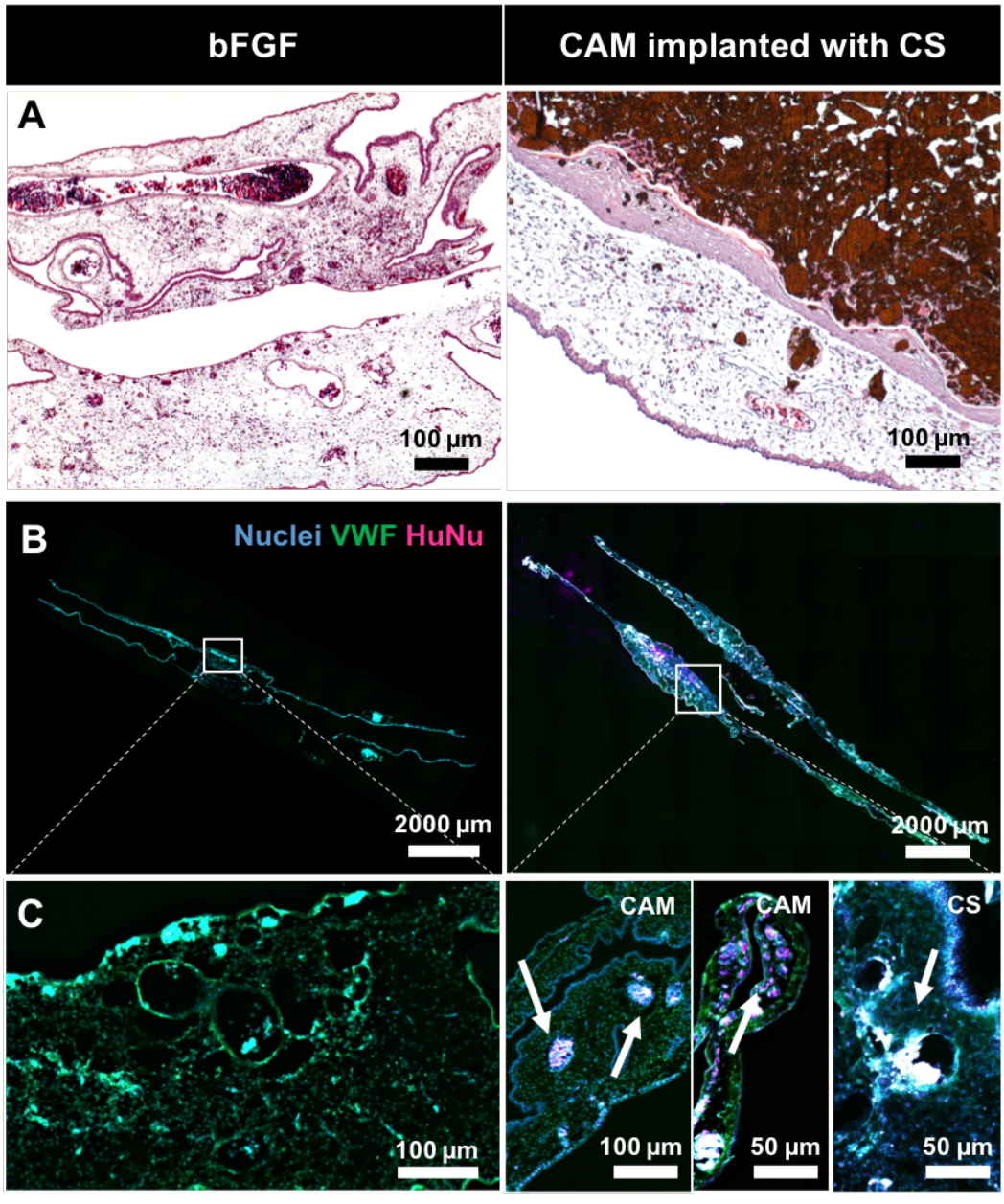

Fig.7 – CS integration within the CAM. (**A)** H&E staining of paraffin-embedded CAMs; (**B)** Immunostaining of CAM with implanted CS and CAM implanted with bFGF (positive control). VWF (in green) labels both human and chick endothelial cells, DAPI (in blue) stains all nuclei, and HuNu (in pink) stains the human nuclei. (**C)** Zoom of CAMs sections. As displayed in CAM with implanted CS, human nuclei are integrated within the CAM and have integrated chick vasculature (white arrows). The presence of human vessels within the CS is also corroborated by the overlapping of HuNu and VWF (white arrow).

4. Discussion

One of the major hurdles in fabricating 3D tissues from CSs involved the engineering of mechanically resistant cell-constructs for vascularized tissues. The poor mechanical properties of CSs monolayers can be overcome through the construction of thicker ones. However, the thickness limitation of multilayered CSs is correlated with the need for blood vessels supplying oxygen and essential nutrients throughout the 3D construct,[5,10] while removing metabolic waste.[38] In fact, thick and highly-dense CSs without blood vessels have already been reported to be unable to survive *in vivo*.[10] It has also been reported that the lack of adequate vascularization induces necrosis in tissues thicker than 100-200μm.[9,38] To overcome such limitations pre-vascularization strategies have been used to accelerate its perfusion after CS implantation, guarantying the survival of the 3D construct and the correct interaction with the host tissue. [5,7,10,11,38–41]

The works reported in the literature regarding the establishment of pre-vascularized CS consist on the individual stacking of previously formed CS monolayers by making use of thermo-responsive surfaces. To aid in such CS fabrication, Okano and co-workers have proposed a methodology that encompasses the use of a CS layering manipulator that avoids the shrinkage of the developed CS after detachment from the thermo-responsive surfaces. Such devices have been used to lift up to three CS monolayers from individual PIPAAm surfaces,[19,38] yet the ability to lift up to ten monolayers is reported.[5] However, this manipulation requires skills and user-knowledge to successful deposit the CS into layers. To overcome this limitation the same researchers have developed an automatic apparatus able to stack several CSs in a reproducible manner without requiring the expertise of the operator. Nevertheless, the cost for the fabrication of the apparatus and the need for a clean room facility make the process unsuitable for most research facilities. In addition, PIPAAm thermo-responsive surfaces are also known to exhibit some limitations such as high cost, abnormal cellular activity due to physiological alteration within cell microenvironment and restrains in tissue replacement.[42] Also, the spatial control of the positioning of target cells is challenging in such approach.[21] In Mag-TE, cells are labeled with magnetic biocompatible nanoparticles and forced to interact with each other, prompting cell-cell adhesion.[43] In fact, the use of biocompatible magnetite nanoparticles in the TE and regenerative field has long been proven to provide outstanding biological and medical applications.[43–46] Mag-TE technology has been used to produce heterotypic CS of HAECs and human hepatocytes with satisfactory outcomes.[1,20,23]

By taking advantage of this expertise, we herein report the development of a stratified and hierarchical 3D vascularized construct to fit bone TE purposes. CS applications towards bone regeneration using thermo-responsive surfaces have already been proposed.[7–9,47] In published studies, a co-culture of endothelial cells and bone marrow derived stromal cells (hBMSCs) was performed in culture media supplemented with osteogenic factors such as dexamethasone and ascorbic acid. Pirraco *et al.* and Mendes *et al.* stacked such co-cultured layers with a layer of hBMSCs. In turn, Ren *et al.* and Li *et al.* folded the co-cultured CS construct to create a 3D vascularized tissue. [8,17,33,48] Recently, Zhang *et al.* created a double CS complex through the stacking of previously differentiated ASCs into either osteogenic CSs or endothelial CSs. The

authors investigated the influence of stacking both layers in different orders and, in further conjugation with a coral hydroxyapatite scaffold, assessed the newly formed vessels after subcutaneous heterotypic transplantation in nude mice. Again, the contractile nature of such CS hinders the manipulation of the construct.[30]

Here, we proposed the developed of a pre-vascularized heterotypic CS by making use of Mag-TE technology, in simple, one-pot, cost effective and time-saving fashion. By magnetically pushing both heterotypic and homotypic cell-cell interactions we attempted to easily create a fully functional pre-vascularized tissue, and to demonstrate the synergic interaction between HUVECs and ASCs, as well as the self-generation of growth factors and proteins that boost both osteo- and angiogenesis in the developed tissue construct. Thus, we hypothesized that our endothelized magnetically labeled CS could coordinate the precise signals towards new bone formation without requiring the supplementation of the three main osteogenic differentiation factors, such as dexamethasone, ascorbic acid and β-glycerophosphate, while exhibiting angiogenic potential both *in vitro* and *in vivo*. Such hypothesis is in line with other studies and emphasizes the potential use of endothelial cells in the osteogenic differentiation of ASCs, when compared to the monoculture counterparts. [6,13,49,50]

In this sense, ASCs and HUVECs were successfully labeled with magnetic nanoparticles. Homotypic ASCs CS and heterotypic CSs comprising of an HUVECs CS in between two ACSs CSs, were engineered as described above. An identical number of ASCs was used for both assemblies. With the aid of magnetic force, cell-cell homotypic and heterotypic interactions were enforced, enabling the development of a cohesive and stratified tissue. In addition, visual perception of both CS constructs revealed that a more cohesive CS was obtained for the heterotypic condition. CS integrity in both homotypic and heterotypic tissues was corroborated via SEM imaging and by H&E staining, where *de novo* matrix was also identified. Cell-cell interactions in the heterotypic CS were corroborated through vinculin orange-staining. An immunodetection of CD31 confirmed the presence of a CS of HUVECs in between the two CSs of ASCs, as demonstrated by the side sections of the confocal image. The cross talk between ASCs and HUVECs was confirmed through CS osteogenic differentiation. Thick and collagen-enriched matrices were achieved in heterotypic CS for both culture media conditions. The metabolic activity stagnation together with ALP/DNA increase in the heterotypic stratified CS and monotypic CS cultured in osteogenic media also suggested osteogenic differentiation. Moreover, ALP, which is secreted by active osteoblasts, is known to cleave the pyrophosphate ions that hamper the formation of hydroxyapatite crystals. Such ALP-induced hydrolysis results in the saturation of the extracellular fluid with orthophosphates that stimulate matrix mineralization.[13,51,52] This has been well-documented by the calcium deposition, hydroxyapatite crystals and Ca/P ratio approaching the one found in cortical bone.[31,32] The obtained results for ALP and hydroxyapatite deposition also suggest a delay in osteogenesis for the homotypic CS when compared to the heterotypic CS cultured in osteogenic conditions. Such effect was already expected as the combination of both strategies triggers a faster osteogenic differentiation.[13]

The pro-osteogenic potential of CS was also evaluated through the secretion of the two major non-collagenous proteins osteopontin and osteocalcin, involved in bone matrix organization and deposition. Both proteins are secreted by bone differentiated cells and are produced during bone formation, late in the mineralization process controlling mass, mineral size and orientation, regulating whole-bone structure and morphology.[53] The results suggested osteogenic differentiation in both heterotypic and homotypic CSs cultured under the influence of osteogenic factors, suggesting a similar effect for these factors and endothelial cells in the expression of this non-collagenous proteins. Residual osteopontin expression was also achieved for ASCs monoculture CS. Osteocalcin secretion follows a similar tendency. Nevertheless, as osteocalcin

is only expressed by active osteoblasts, the differences between conditions appear to be more pronounced, as the osteocalcin expression in ASCs is negligent. Such effect re-suggests a seven-day late osteogenic differentiation in the homotypic CS cultured under osteogenic factors and in the heterotypic CS cultured in the absence of those components (basal media). Immunodetection of all forms of osteopontin in both heterotypic CS revealed a similar fluorescence intensity after 21 days of culture.

As has been widely reported, osteogenesis and vascularization are coupled during bone development and growth. In fact, angiogenesis is known to play a fundamental role in bone growth and remodeling.[7,8,13,17,33,35] VEGF and BMP-2 have been widely used in TE and regenerative medicine to synergically incite angiogenesis and bone formation.[54] VEGF, which is known to be expressed in ASCs,[13,55] is a strong angiogenic factor, and plays a fundamental role in blood vessel invasion and in the secretion of growth factors that stimulate osteogenesis[35]. On the other hand, BMP-2 is an osteogenic growth factor that is involved in improved bone tissue regeneration,[13,56–59] is expressed in several cell types including endothelial ones. The ability of endothelial cells to release BMP-2 by the action of VEGF is well document in the literature and supports our findings. As expected, pre-vascularized heterotypic CS secrete more BMP-2. Moreover, the synergic effect of the co-culture together with the differentiating osteogenic factors resulted in a higher BMP-2 release, measure at the end of the experiment (21 days). Nevertheless, the results confirm that the co-culture of endothelial cells and ASCs was sufficient to induce the release of BMP-2, since the amount released is higher than the one evidenced in homotypic CS. Also, the crosstalk between BMP-2 and VEGF was likewise corroborated by the VEGF release. As time increased and upon osteogenic differentiation (evidenced by BMP-2, osteopontin, osteocalcin, ALP and Ca/P ratio increase overtime), ASCs capability to induce angiogenesis is diminished, which in turn down-regulated VEGF expression. Equivalent results were evidenced in a co-culture of microvascular endothelial cells and ASCs within a 3D system of liquified capsules.[13] Similarly, the delayed osteogenesis observed for the heterotypic CS cultured in the absence of osteogenic factors, could in fact represent an added value. In fact, the amount of VEGF being released may further trigger the recruitment of new vessels, enhancing angiogenesis and enabling the formation of a more vascularized osteogenic tissue. In light of such events, the angiogenic potential of the heterotypic CS cultured under basal conditions was investigated. After 21 days of *in vitro* culture, the developed CSs revealed the presence of vascular structures, which was corroborated through i) the combination of CD31 (endothelial cells' marker) and the deposition of the basement membrane protein collagen IV; and ii) the association of FN, that is particularly relevant during blood vessel formation and VWF (another endothelial cells' marker). The *in vivo* angiogenic potential of heterotypic CS cultured in basal medium for 7 days was also investigated through a CAM assay,[37] and compared to the effect of the angiogenic stimulant bFGF.[60] The number of new capillaries formed around the implantation area suggests a similar performance between the heterotypic CS and the positive control, only 4 days after the CS implantation, likely due to the increased VEGF levels during that period. Human cells showed to be able to migrate into the host and integrate chick vasculature as corroborated by H&E staining, where MNPs have integrated the CAM and its vasculature, as well as by the presence of a specific human nuclei marker. Moreover, the presence of human vessels in the CAM chick and in our CS was identified by the overlapping of HuNu with VWF. Although this preliminary *in vivo* angiogenic assay demonstrated that our magnetically labeled heterotypic CSs stimulates blood vessels recruitment and integration within the host environment, forthcoming studies including the implementation of this CS in more realistic models for clinical applications, where angiogenesis and *de novo* bone formation could be fully evaluated. With this technology, we intend to create personalized CSs with patient own cells. Although we suggest using endothelial

cells from umbilical cord source, in case of impossibility, human adipose microvascular endothelial cells (ECs) can be retrieved from adipose tissue. As already demonstrated in the group, the combination ASCs and ECs is also expected to produce bone-like tissues under similar conditions.[13] IPSC technology may also be used to create patient-specific CSs. In fact, the tremendous potential of IPSC in regenerative medicine, particularly in the development CSs for heart, liver and retinal therapies, has already been disclosed.[61–63] The developed CSs can be used as membranes for guided bone regeneration either by placing the CSs on top of cranial or maxillofacial defects, or by wrapping around femoral bone injury.[64] In fact, CSs for bone regeneration are commonly used as membranes for periosteum repair, a highly vascularized tissue that resides in a dynamic mechanically loaded environment and envelopes the bone surface of long bones.[65] Even though this study focused on bone regeneration, we believe that the easiness of the methodology herein describe could be extended to further applications for a plethora of hierarchical tissues by adapting the cell phenotypes within the fabricated CS.

5. Conclusion

Mag-TE has shown remarkable outcomes in the fabrication of both homotypic and heterotypic CS in a simple, one-pot, cost-effective and time-saving manner, enabling the construction and manipulation with the aid of mild magnetic force. Stimulated by the high vascularization nature of bone tissue, we herein developed a hierarchical 3D cohesive tissue of HUVECs and ASCs based on CS technology and Mag-TE, to be used in bone regeneration purposes. The hierarchical construct (ASCs/HUVECs/ASCs) revealed to be effective in stimulating *in vitro* osteogenesis through the crosstalk of both cells' phenotypes, even in the absence of osteogenic differentiating factors such as dexamethasone, ascorbic acid and β-glycerophosphate. Furthermore, VEGF and BMP-2 release triggered the recruitment of more blood vessels, empowering the outstanding potential of the developed system for TE practices. The development of pre-vascularized/angiogenic magnetically actuated CS is expected to improve to a great extent the use of such technology in the creation of robust and easily manipulated cell constructs to fit TE purposes.

Acknowledgments

We acknowledge the project CICECO – Aveiro Institute of Materials, POCI-01-0145-FEDER-007679 [Fundação para a Ciência e Tecnologia (FCT) Ref. UID/CTM/50011/2013], financed by national funds through the FCT/Ministério da Educação e Ciência, and PROMENADE (Ref. PTDC/BTM-MAT/29830/2017). This work was also supported by the project ATLAS (ref.ERC-2014-ADG-669858) and through the doctoral grants SFRH/BD/141523/2018 (Lúcia F. Santos) and SFRH/BD/146740/2019 (Maria C. Mendes).
Confocal image acquisition was performed in the LiM facility of iBiMED, a node of PPBI (Portuguese Platform of BioImaging): POCI-01-0145-FEDER-022122. We also acknowledge to Marta Teixeira Pinto for the CAM assay technique performed at the "*in vivo* CAM assays" i3S Scientific Platform and for the helpful discussions.

Data availability

The raw/processed data required to reproduce these findings cannot be shared at this time as the data also forms part of an ongoing study.

References

(1) Ito, A.; Jitsunobu, H.; Kawabe, Y.; Kamihira, M. Construction of Heterotypic Cell Sheets by Magnetic Force-Based 3-D Coculture of HepG2 and NIH3T3 Cells. *J. Biosci. Bioeng.* **2007**, *104*, 371–378.

(2) Yang, J.; Yamato, M.; Kohno, C.; Nishimoto, A.; Sekine, H.; Fukai, F.; Okano, T. Cell Sheet Engineering: Recreating Tissues without Biodegradable Scaffolds. *Biomaterials* **2005**, *26*, 6415–6422.

(3) Yamato, M.; Okano, T. Cell Sheet Engineering. *Mater. Today* **2004**, *7*, 42–47.

(4) Yang, J.; Yamato, M.; Shimizu, T.; Sekine, H.; Ohashi, K.; Kanzaki, M.; Ohki, T.; Nishida, K.; Okano, T. Reconstruction of Functional Tissues with Cell Sheet Engineering. **2007**, *28*, 5033–5043.

(5) Owaki, T.; Shimizu, T.; Yamato, M.; Okano, T. Cell Sheet Engineering for Regenerative Medicine : Current Challenges and Strategies. *Biotechnol. J.* **2014**, *9*, 904–914.

(6) Costa, M.; Cerqueira, M. T.; Santos, T. C.; Sampaio-Marques, B.; Ludovico, P.; Marques, A. P.; Pirraco, R. P.; Reis, R. L. Cell Sheet Engineering Using Stromal Vascular Fraction of Adipose Tissue as a Vascularization Strategy. *Acta Biomater.* **2017**, *55*, 131–143.

(7) Pirraco, P.; Iwata, T.; Yoshida, T.; Marques, A. P.; Yamato, M.; Reis, R. L. Endothelial Cells Enhance the in Vivo Bone-Forming Ability of Osteogenic Cell Sheets. *Lab. Investig.* **2014**, *94*, 663–673.

(8) Mendes, L. F.; Pirraco, P.; Szymczyk, W.; Frias, A. M.; Santos, T. C.; Reis, R. L.; Marques, A. P. Perivascular-Like Cells Contribute to the Stability of the Vascular Network of Osteogenic Tissue Formed from Cell Sheet-Based Constructs. *PLoS One* **2012**, *7*, 1–12.

(9) Moschouris, K.; Firoozi, N.; Kang, Y. The Application of Cell Sheet Engineering in the Vascularization of Tissue Regeneration. *Regen. Med.* **2016**, *11*, 559–570.

(10) Sekine, W.; Haraguchi, Y.; Shimizu, T.; Umezawa, A.; Okano, T. Thickness Limitation and Cell Viability of Multi-Layered Cell Sheets and Overcoming the Diffusion Limit by a Porous-Membrane Culture Insert. *J. Biochips Tissue chips* **2011**, *S1:007*.

(11) Hong, S.; Young, B.; Changmo, J. Multilayered Engineered Tissue Sheets for Vascularized Tissue Regeneration. *Tissue Eng. Regen. Med.* **2017**, *14*, 371–381.

(12) Lopes, D.; Martins-Cruz, C.; Oliveira, M. B.; Mano, J. F. Bone Physiology as Inspiration for Tissue Regenerative Therapies. *Biomaterials*, **2018,** *185*, 240–275.

(13) Correia, C. R.; Pirraco, R. P.; Cerqueira, M. T.; Marques, A. P.; Reis, R. L.; Mano, J. F. Semipermeable Capsules Wrapping a Multifunctional and Self-Regulated Co-Culture Microenvironment for Osteogenic Differentiation. *Sci. Rep.* **2016**, *6*, 21883.

(14) Amini, A. R.; Laurencin, C. T.; Nukavarapu, S. P. Bone Tissue Engineering: Recent Advances and Challenges. *Crit. Rev. Biomed. Eng.* **2012**, *40*, 363–408.

(15) Rouwkema, J.; Khademhosseini, A. Trends in Biotechnology. *Trends Biotechnol.* **2016**, *34*, 734–745.

(16) Rouwkema, J.; Boer, J. De; Blitterswijk, C. A. Van. Endothelial Cells Assemble into a 3-Dimensional Prevascular Network in a Bone Tissue Engineering Construct. *Tissue Eng.* **2006**, *12*, 2685–2693.

(17) Ren, L.; Kang, Y.; Browne, C.; Bishop, J.; Yang, Y. Fabrication, Vascularization and Osteogenic Properties of a Novel Synthetic Biomimetic Induced Membrane for the Treatment of Large Bone Defects Liling. *Bone* **2015**, *64*, 173–182.

(18) Mano, F.; Reis, R. L.; Silva, R. M. P. Smart Thermoresponsive Coatings and Surfaces for Tissue Engineering : Switching Cell-Material Boundaries. *Trends Biotechnol.* **2007**, *25*, 12–15.

(19) Yamada, N.; Okano, T.; Sakai, H.; Karikusaa, F.; Sawasaki, Y.; Sakurai, Y. Thermo-Responsive Polymeric Surfaces ; Control of Attachment and Detachment of Cultured Cells. *Macromol. Rapid Commun.* **1990**, *576*, 571–576.

(20) Ito, A.; Takizawa, Y.; Honda, H.; Hata, K.; Kagami, H.; Ueda, M.; Kobayashi, T. Construction and Harvest of Multilayered Keratinocyte Sheets Using Magnetite Nanoparticles and Magnetic Force. *Tissue Eng.* **2004**, *10*, 873–880.

(21) Dobson, J. Remote Control of Cellular Behaviour with Magnetic Nanoparticles. *Nature Nanotechnology*, **2008**, *3*, 139–143.
(22) Goncalves, A. I.; Miranda, M. S.; Rodrigues, M. T.; Reis, R. L.; Gomes, M. E. Magnetic Responsive Cell-Based Strategies for Diagnostics and Therapeutics. *Biomedical Materials (Bristol)*, 2018, *13*, 54001.
(23) Ito, A.; Takizawa, Y.; Honda, H.; Hata, K.; Kagami, H.; Ueda, M.; Kobayashi, T. Tissue Engineering Using Magnetite Nanoparticles and Magnetic Force: Heterotypic Layers of Cocultured Hepatocytes and Endothelial Cells. *Tissue Eng.* **2004**, *10*, 833–840.
(24) Gil, S.; Correia, C. R.; Mano, J. F. Magnetically Labeled Cells with Surface-Modified Fe3O4 Spherical and Rod-Shaped Magnetic Nanoparticles for Tissue Engineering Applications. *Adv. Healthc. Mater.* **2015**, *4*, 883–891.
(25) Baudin, B.; Bruneel, A.; Bosselut, N.; Vaubourdolle, M. A Protocol for Isolation and Culture of Human Umbilical Vein Endothelial Cells. *Nat. Protoc.* **2007**, *2*, 481–485.
(26) Kadam, S. S.; Tiwari, S.; Bhonde, R. R. Simultaneous Isolation of Vascular Endothelial Cells and Mesenchymal Stem Cells from the Human Umbilical Cord. *Vitr. Cell. Dev. Biol. - Anim.* **2009**, *45*, 23–27.
(27) Nowak-sliwinska, P.; Ballini, J.; Wagnières, G.; Bergh, H. Van Den. Processing of Fl Uorescence Angiograms for the Quanti Fi Cation of Vascular Effects Induced by Anti-Angiogenic Agents in the CAM Model. *Microvasc. Res.* **2010**, *79*, 21–28.
(28) Bayrakcı, M.; Maltaş, E.; Yiğiter, Ş.; Özmen, M. Synthesis and Application of Novel Magnetite Nanoparticle Based Azacrown Ether for Protein Recognition. *Macromol. Res.* **2013**, *21*, 1029–1035.
(29) Coates, J. Interpretation of Infrared Spectra, A Practical Approach. In *Encyclopedia of Analytical Chemistry*; Meyers, R.; McKelvy, M., Eds.; John Wiley & Sons, Inc., Chichester, **2006**.
(30) Zhang, H.; Zhou, Y.; Zhang, W.; Wang, K.; Xu, L.; Ma, H.; Deng, Y. Construction of Vascularized Tissue-Engineered Bone with a Double-Cell Sheet Complex. *Acta Biomater.* **2018**, *77*, 212–227.
(31) T, B. W.; Pasteris, J. D. A Mineralogical Perspective on the Apatite in Bone. **2005**, *25*, 131–143.
(32) Raynaud, S.; Champion, E. Calcium Phosphate Apatites with Variable Ca / P Atomic Ratio II . Calcination and Sintering. **2002**, *23*, 1073–1080.
(33) Pirraco, R. .; Melo-Ferreira, B.; Santos, T. C.; Frias, A. M.; Marques, A. P.; Reis, R. L. Adipose Stem Cell-Derived Osteoblasts Sustain the Functionality of Endothelial Progenitors from the Mononuclear Fraction of Umbilical Cord Blood. *Acta Biomater.* **2013**, *9*, 5234–5242.
(34) Tumarkin, E.; Lsan, T.; Csaszar, E.; Seo, M.; Zhang, H.; Lee, A.; Peerani, R.; Purpura, K.; Zandstra, P. W.; Kumacheva, E. High-Throughput Combinatorial Cell Co-Culture Using Microfluidics. *Integr. Biol.* **2011**, *3*, 653–662.
(35) Hu, K.; Olsen, B. R. The Roles of Vascular Endothelial Growth Factor in Bone Repair and Regeneration. *System* **1967**, *91*, 30–38.
(36) Barati, D.; Ramin, S.; Shariati, P.; Moeinzadeh, S.; Melero-, J. M.; Khademhosseini, A.; Jabbari, E. Spatiotemporal Release of BMP-2 and VEGF Enhances Osteogenic and Vasculogenic Differentiation of Human Mesenchymal Stem Cells and Endothelial Colony-Forming Cells Co-Encapsulated in a Patterned Hydroge. *J. Control. Release* **2017**, *223*, 126–136.
(37) Torres, A. L.; Bidarra, S. J.; Pinto, M. T.; Aguiar, P. C.; Silva, E. A.; Barrias, C. C. Guiding Morphogenesis in Cell-Instructive Microgels for Therapeutic Angiogenesis. *Biomaterials* **2018**, *154*, 34–47.
(38) Asakawa, N.; Shimizu, T.; Tsuda, Y.; Sekiya, S.; Sasagawa, T.; Yamato, M.; Fukai, F.; Okano, T. Pre-Vascularization of in Vitro Three-Dimensional Tissues Created by Cell Sheet Engineering. *Biomaterials* **2010**, *31*, 3903–3909.
(39) Costa, M.; Cerqueira, M. T.; Santos, T. C.; Sampaio-Marques, B.; Ludovico, P.; Marques, A. P.; Pirraco, R. P.; Reis, R. L. Cell Sheet Engineering Using the Stromal Vascular Fraction of Adipose Tissue as a Vascularization Strategy. *Acta Biomater.* **2017**,

55, 131–143.
(40) Sekiya, S.; Muraoka, M.; Sasagawa, T.; Shimizu, T.; Yamato, M.; Okano, T. Three-Dimensional Cell-Dense Constructs Containing Endothelial Cell-Networks Are an Effective Tool for in Vivo and in Vitro Vascular Biology Research. *Microvasc. Res.* **2010**, *80*, 549–551.
(41) Takeuchi, R.; Kuruma, Y.; Sekine, H.; Dobashi, I.; Yamato, M.; Umezu, M.; Shimizu, T.; Okano, T. In Vivo Vascularization of Cell Sheets Provided Better Long-Term Tissue Survival than Injection of Cell Suspension. *J. Tissue Eng. Regen. Med.* **2016**, *10*, 700–710.
(42) Kim, I. Y.; Iwatsuki, R.; Kikuta, K.; Morita, Y.; Miyazaki, T.; Ohtsuki, C. Thermoreversible Behavior of κ-Carrageenan and Its Apatite-Forming Ability in Simulated Body Fluid. *Mater. Sci. Eng. C* **2011**, *31*, 1472–1476.
(43) Castro, E.; Mano, J. F. Magnetic Force-Based Tissue Engineering and Regenerative Medicine. *J. Biomed. Nanotechnol.* **2013**, *9*, 1129–1136.
(44) Gupta, A. K.; Naregalkar, R. R.; Vaidya, V. D.; Gupta, M. Recent Advances on Surface Engineering of Magnetic Iron Oxide Nanoparticles and Their Biomedical Applications. *Nanomedicine* **2007**, *2*, 23–39.
(45) Ito, A.; Shinkai, M.; Honda, H.; Kobayashi, T. Medical Application of Functionalized Magnetic Nanoparticles. *J. Biosci. Bioeng.* **2005**, *100*, 1–11.
(46) Shubayev, V. I.; Pisanic, T. R.; Jin, S. Magnetic Nanoparticles for Theragnostics. *Adv. Drug Deliv. Rev.* **2009**, *61*, 467–477.
(47) Nakamura, A.; Akahane, M.; Shigematsu, H.; Tadokoro, M.; Morita, Y. Cell Sheet Transplantation of Cultured Mesenchymal Stem Cells Enhances Bone Formation in a Rat Nonunion Model. *Bone* **2010**, *46*, 418–424.
(48) Liu, H.; Zhou, W.; Ren, N.; Feng, Z.; Dong, Y.; Bai, S.; Jiao, Y. Cell Sheets of Co-Cultured Endothelial Progenitor Cells and Mesenchymal Stromal Cells Promote Osseointegration in Irradiated Rat Bone. **2017**, 1–12.
(49) Lee, K.; Silva, E. A.; Mooney, D. J. Growth Factor Delivery-Based Tissue Engineering : General Approaches and a Review of Recent Developments. **2011**, 153–170.
(50) Baldwin, J.; Antille, M.; Bonda, U.; De-Juan-Pardo, E. M.; Khosrotehrani, K.; Ivanovski, S.; Petcu, E.; Hutmacher, D. In Vitro Pre-Vascularisation of Tissue-Engineered Construct: A Co-Culture Perspective. *Vasc. Cell* **2014**, *6*, 13.
(51) Grover, L. M.; Wright, A. J.; Gbureck, U.; Bolarinwa, A.; Song, J.; Liu, Y.; Farrar, D. F.; Howling, G.; Rose, J.; Barralet, J. E. Biomaterials The Effect of Amorphous Pyrophosphate on Calcium Phosphate Cement Resorption and Bone Generation. *Biomaterials* **2013**, *34*, 6631–6637.
(52) Liu, J.; Nam, H. K.; Campbell, C.; Gasque, K. C. da S.; Millán, J. L.; Hatch, N. E. Tissue-Nonspecific Alkaline Phosphatase Deficiency Causes Abnormal Craniofacial Bone Development in the Alpl-/- Mouse Model of Infantile Hypophosphatasia. *Bone* **2014**, *67*, 81–94.
(53) Bailey, S.; Karsenty, G.; Gundberg, C.; Vashishth, D.; Haven, N. Osteocalcin and Osteopontin Influence Bone Morphology and Mechanical Properties. **2018**, *1409*, 79–84.
(54) Zhang, W.; Zhu, C.; Wu, Y.; Ye, D.; Wang, S.; Zou, D.; Zhang, X.; Kaplan, D.; Jiang, X. VEGF and BMP-2 Promote Bone Regeneration by Facilitating Bone Marrow Stem Cell Homing and Differentiation. *Eur. Cells Mater.* **2016**, *27*, 1–12.
(55) Verseijden, F.; Jahr, H.; Posthumus-van Sluijs, S. J.; Hagen, T. L. T. Ten; Hovius, S. E. R.; Seynhaeve, A. L. B.; van Neck, J. W.; van Osch, G. J. V. M.; Hofer, S. O. P.; Hovious, S. E. R.; *et al.* Angiogenic Capacity of Human Adipose-Derived Stromal Cells During Adipogenic Differentiation: An In Vitro Study. *Tissue Eng. - Part A* **2008**, *15*, 445–452.
(56) Marupanthorn, A.; Tantrawatpan, C.; Kheolamai, P.; Tantikanlayaporn, D.; Manochantr, S. Bone Morphogenetic Protein-2 Enhances the Osteogenic Differentiation Capacity of Mesenchymal Stromal Cells Derived from Human Bone Marrow and Umbilical Cord. *Int. J. Mol. Med.* **2017**, *39*, 654–662.
(57) Thébaud, N. B.; Siadous, R.; Bareille, R.; Remy, M.; Daculsi, R.; Amédée, J.;

Bordenave, L. Whatever Their Differentiation Status, Human Progenitor Derived – or Mature – Endothelial Cells Induce Osteoblastic Differentiation of Bone Marrow Stromal Cells. *Tissue Eng. Regen. Med.* **2012**, *6*, e51–e60.

(58) Saleh, F. A.; Whyte, M.; Genever, P. G. Effects of Endothelial Cells on Human Mesenchymal Stem Cell Activity in a Three-Dimensional in Vitro Model. *Eur. Cells Mater.* **2011**, *22*, 242–257.

(59) Leszczynska, J.; Zyzynska-Granica, B.; Koziak, K.; Ruminski, S.; Lewandowska-Szumiel, M. Contribution of Endothelial Cells to Human Bone-Derived Cells Expansio in Coculture. *Tissue Eng. - Part A* **2012**, *19*, 393–402.

(60) Miller, W. J.; Kayton, M. L.; Patton, A.; O'Connor, S.; He, M.; Vu, H.; Baibakov, G.; Lorang, D.; Knezevic, V.; Kohn, E.; *et al.* A Novel Technique for Quantifying Changes in Vascular Density, Endothelial Cell Proliferation and Protein Expression in Response to Modulators of Angiogenesis Using the Chick Chorioallantoic Membrane (CAM) Assay. *J. Transl. Med.* **2004**, *2*, 1–12.

(61) Nagamoto, Y.; Takayama, K.; Ohashi, K.; Okamoto, R.; Sakurai, F.; Tachibana, M.; Kawabata, K.; Mizuguchi, H. Transplantation of a Human IPSC-Derived Hepatocyte Sheet Increases Survival in Mice with Acute Liver Failure. **2016**, *64*, 1–6.

(62) Takagi, S.; Mandai, M.; Hirami, Y.; Kurimoto, Y.; Takahashi, M. Induced Pluripotent Stem Cell-Based Cell Therapy of the Retina. In *Medical Applications of iPS Cells : Innovation in Medical Sciences*; Inoue, H.; Nakamura, Y., Eds.; Springer Singapore: Singapore, **2019;** pp. 133–147.

(63) Kawamura, M.; Miyaga, S.; Fukushima, S.; Saito, A.; Miki, K.; Miyagawa, S.; Fukushima, S.; Saito, A.; Miki, K.; Funakoshi, S.; *et al.* Enhanced Therapeutic Effects of Human IPS Cell Derived-Cardiomyocyte by Combined Cell-Sheets with Omental Flap Technique in Porcine Ischemic Cardiomyopathy Model. *Sci. Rep.* **2017**, *7*, 8824–8824.

(64) Lu, Y.; Zhang, W.; Wang, J.; Yang, G.; Yin, S.; Tang, T.; Yu, C.; Jiang, X. Recent Advances in Cell Sheet Technology for Bone and Cartilage Regeneration : From Preparation to Application. *Int. J. Oral Sci.* **2019**.

(65) Wang, T.; Zhai, Y.; Nuzzo, M.; Yang, X.; Yang, Y.; Zhang, X. Layer-by-Layer Nanofiber-Enabled Engineering of Biomimetic Periosteum for Bone Repair and Reconstruction. *Biomaterials* **2018**, *182*, 279–288.

Supporting Information

Multi-layer vascularized magnetic cell sheets for bone regeneration

Ana S. Silva[1*], Lúcia F. Santos[1], Maria C. Mendes, João F. Mano[*]

1- Both authors had contributed equally to the preparation of the manuscript
* corresponding author: sofiamsilva@ua.pt; jmano@ua.pt

Affiliation: Department of Chemistry, CICECO–Aveiro Institute of Materials, University of Aveiro, 3810-193 Aveiro, Portugal

Contents:

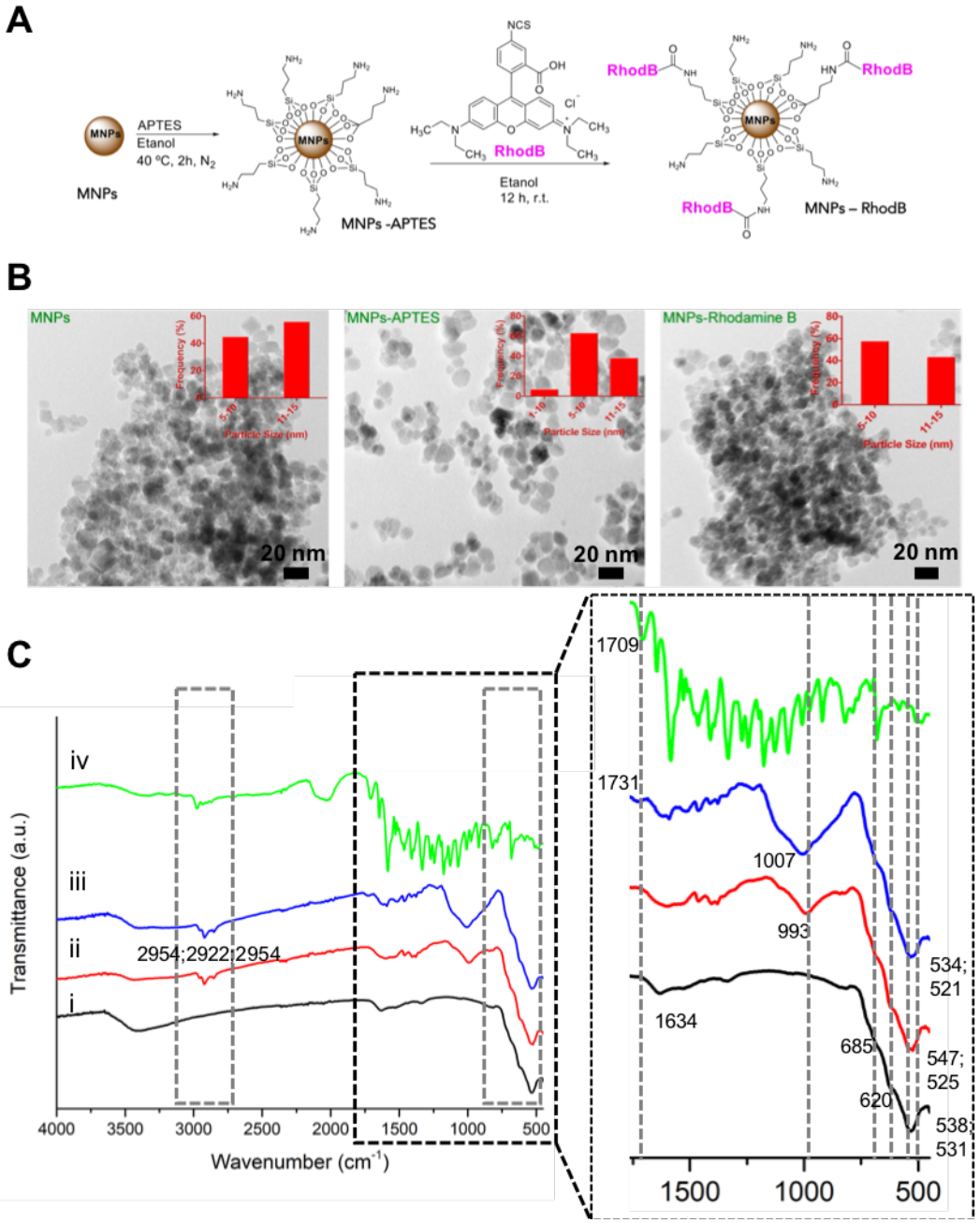

Fig. S1 – Characterization of MNPs. (**A)** Schematic representation of the functionalization of the particles; (**B)** TEM micrographs and size distribution of MNPs and its modifications. (**C)** FTIR-spectra of i) MNPs unmodified; ii) MNPs-APTES; iii) MNPs-RodB; and RodB.

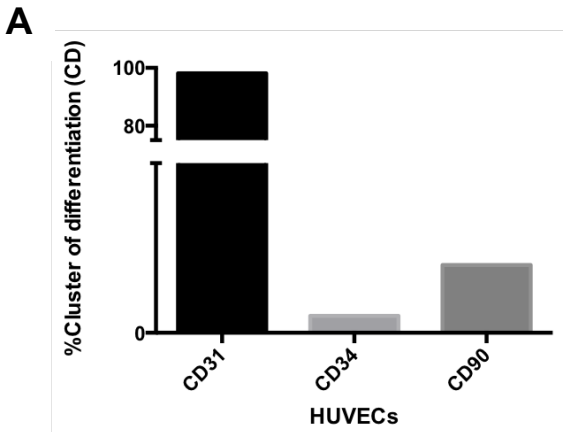

Fig. S2 - Flow cytometry analysis of surface markers expression of HUVECs.

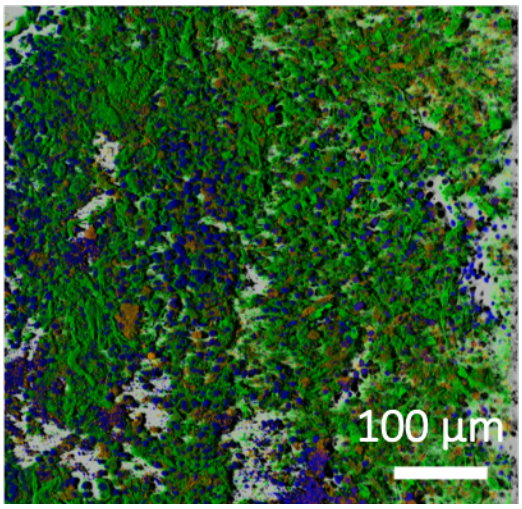

Fig. S3 – Confocal microscopy of vinculin staining in heterotypic CS. After 7 days of culture, the cell-cell and cell-matrix junctions were demonstrated by the presence of vinculin (in orange) in actin cytoskeleton (in green). Cell nuclei are depicted in DAPI (blue).

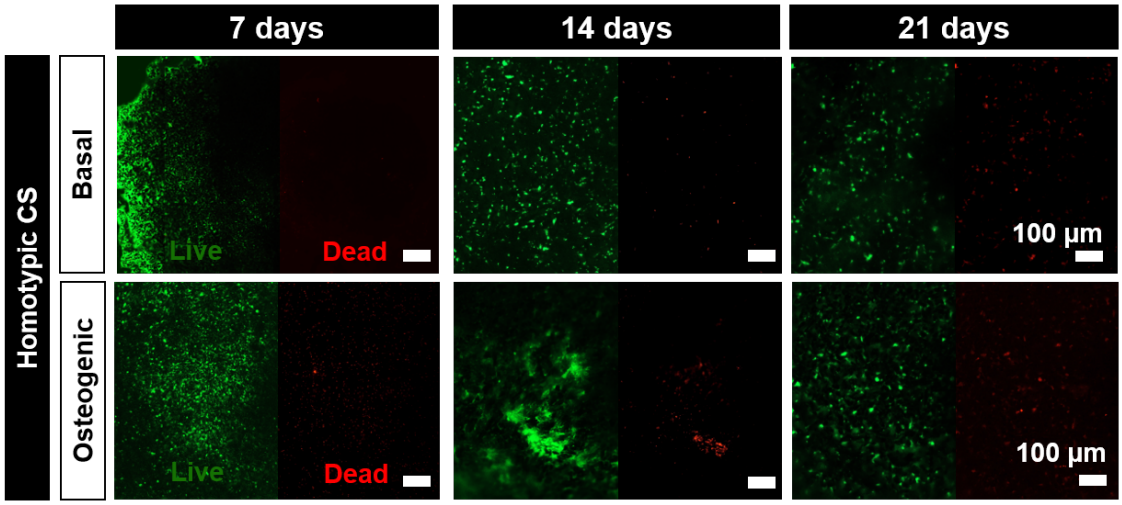

Fig.S4 - Live-dead assay of homotypic CSs. Live-dead fluorescence assay at day 7, 14 and 21 of culture in basal and osteogenic medium. Living cells were stained by calcein (green) and dead cells by propidium iodide (red).

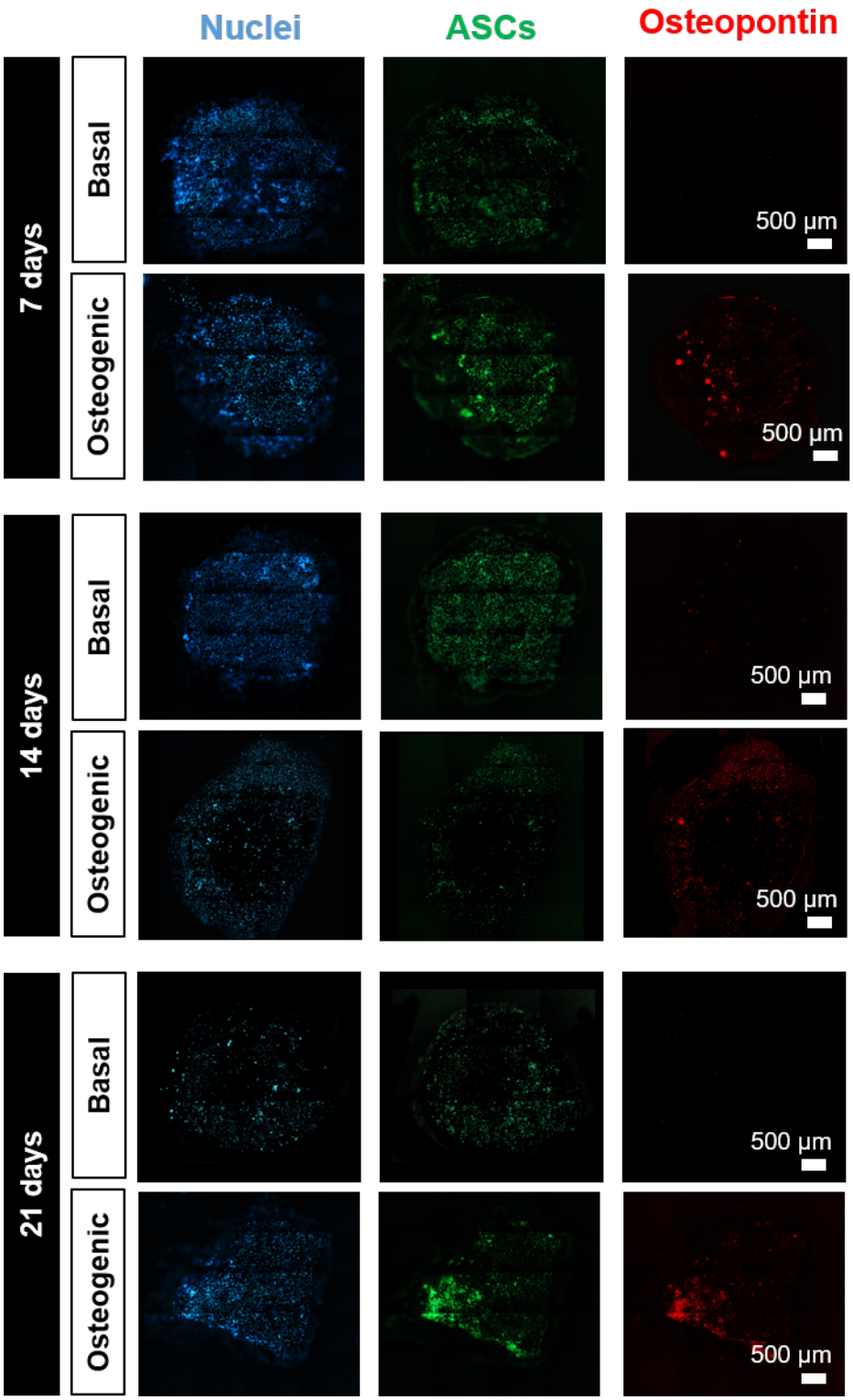

Fig. S5 – Osteopontin staining of homotypic CS. Immunofluorescence of ASCs (green), osteopontin (red) and cell nucleus- DAPI (blue) in 3D homotypic CS cultured for 7, 14 and 21 days in basal and osteogenic media**.**

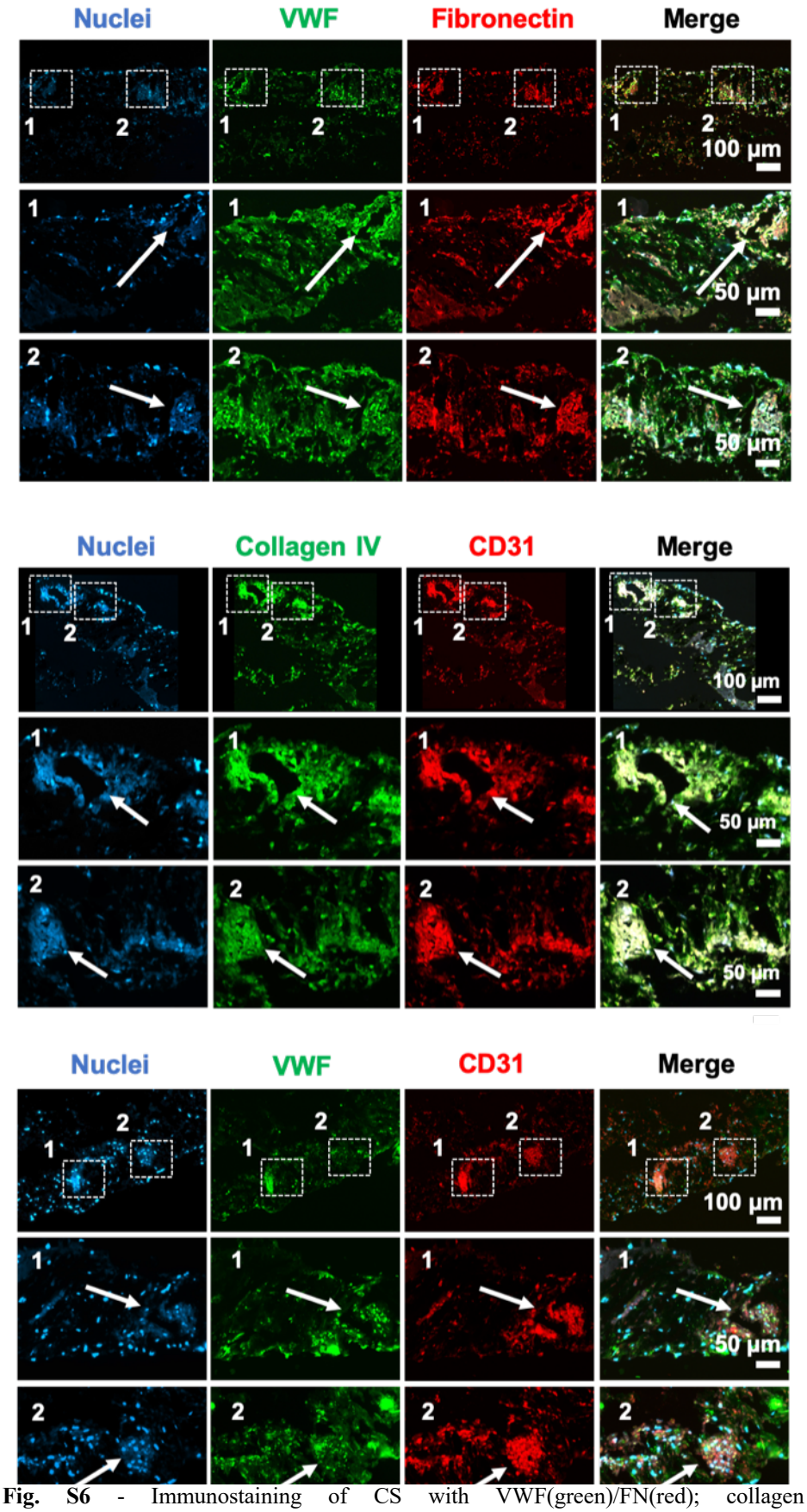

Fig. S6 - Immunostaining of CS with VWF(green)/FN(red); collagen IV(green)/CD31(red) and VWF(green)/CD31(red) demonstrating the presence of capillary-like structures (white arrows). DAPI stains the cells' nuclei.

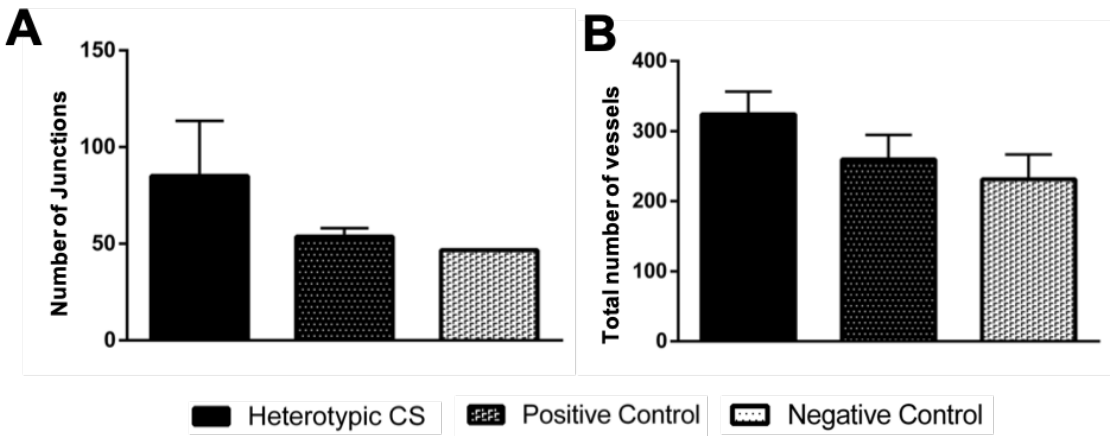

Fig.S7 – Number of junctions (A) and total number of vessels (B). Although higher values were evidenced for the heterotypic CS implanted within the CAM, no significant differences were evidenced.

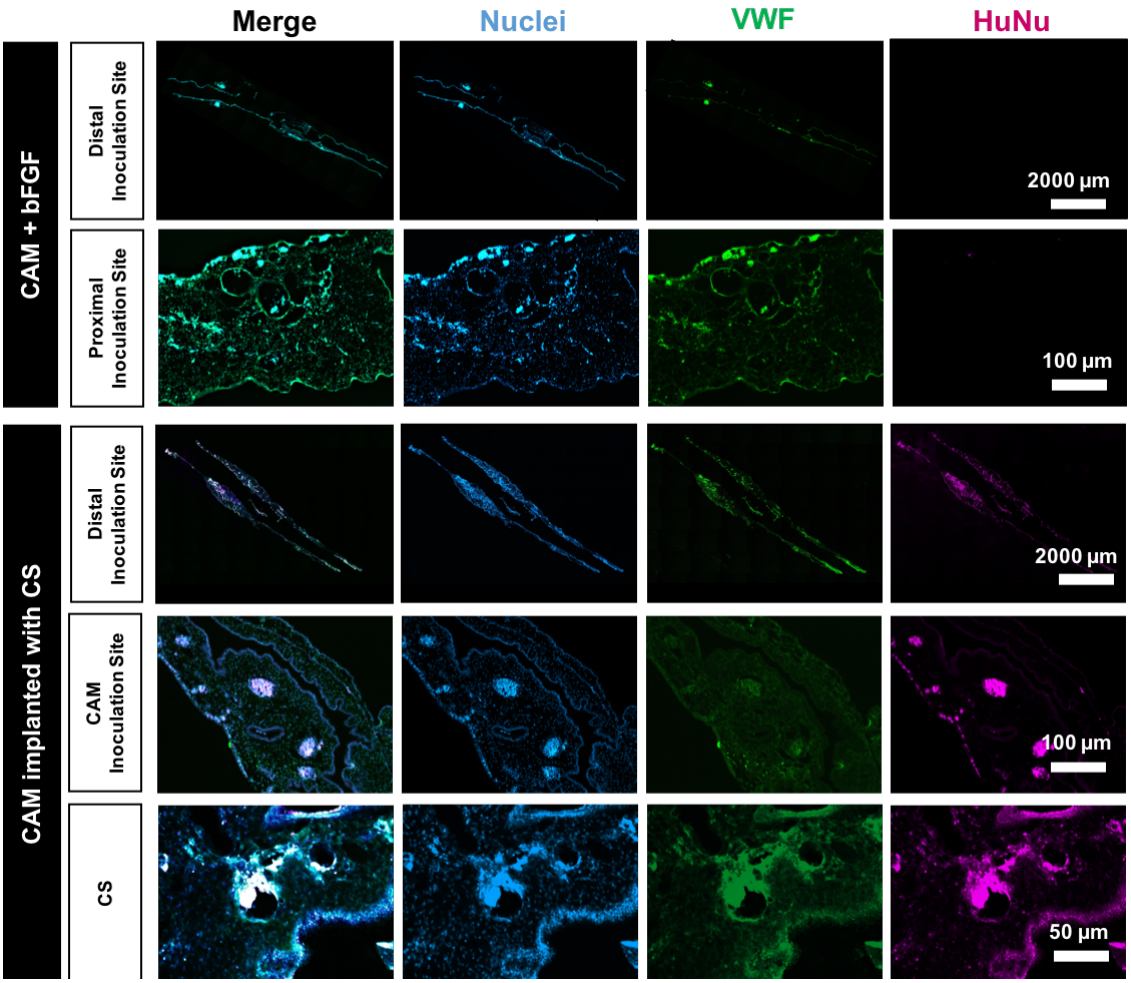

Figure S8– Immunostaining of CAM + bFGF (positive control) and CAM with implanted CS. VWF (in green) labels both human and chick endothelial cells, DAPI (in blue) stains all nuclei, and HuNu (in pink) stains the human nuclei. As displayed, human nuclei are integrated within the CAM and have integrated chick vasculature corroborated by the overlapping of VWF and HuNu stainings.